

(!) PREPRINT VERSION (!)

Creative Commons license: CC BY-NC-ND 4.0 (<https://creativecommons.org/licenses/by-nc-nd/4.0/>)

When citing this research, please refer to the final version of this book chapter (which was only slightly modified with respect to this preprint version):

Zwaan, F., Schreurs, G. (*in press*). Analogue modelling of continental rifting: an overview, In: Peron-Pinvidic (ed.): *Rifted Margins*, ISTE-WILEY.

Please feel free to contact the authors for information (or a copy of the final version)

Analogue modelling of continental rifting: an overview

Frank Zwaan^a, Guido Schreurs^a

(a) University of Bern, Baltzerstrasse 1+3, 3012 Switzerland
email: frank.zwaan@geo.unibe.ch

Keywords: Continental rifting, analogue modelling, extension, experimental modelling, analysis techniques, rift propagation, rift interaction, oblique extension

1. Introduction

When studying rifts and rifted margins, geologists have to face various challenges. Such tectonic systems cover large parts of the globe, making it hard to chart them in detail. Furthermore, large parts of these systems are buried under thick layers of sediment or covered by water, strongly reducing their accessibility. These problems have been mitigated to a degree by the use of geophysical techniques, in particular reflection seismics, and deep borehole drilling. Yet perhaps the greatest obstacle on the path to a thorough understanding of rift processes is posed by the timescale on which the latter operate. It is simply not possible to directly observe the development of a rift system that takes millions of years, and the processes and kinematics involved remain obscure.

Recognizing these challenges, geologists have long since turned to analogue models. By choosing the correct materials and experimental set-up, it is possible to simulate tectonic processes stretching over vast spatial and temporal scales within a couple of hours or days in the laboratory. This approach provides an easy and relatively cheap method to test various parameters that may affect tectonic systems, providing unique insights in associated dynamics and kinematics that are not readily deduced from static field examples, which is especially relevant for petroleum geologists (e.g. Naylor et al. 1994; Brun & Fort 2004). The first such analogue model (or experiment), simulating tectonic folding, was published by Sir James Hall in 1815 (Hall, 1815). In the 200 years since these first experiments, a wide variety of methods have been used to simulate a vast spectrum of tectonic processes (e.g. Graveleau et al. 2012; Koyi 1997). It must however be stressed that analogue modelling applications are not restricted to tectonics, but have also been applied to study, for instance, sedimentary processes, magmatic events, slope collapse and tsunami hazards (e.g. Donnadieu et al. 2003; Wang et al. 2014; McFall & Fritz 2016; Poppe et al. 2019). Meanwhile, a broad arsenal of methods has been developed to not only observe, but also quantify external and internal model deformation, so that the analogue modelling community remains at the forefront of geological innovation.

Although the first models were conducted to simulate compressional tectonics, numerous experimental studies have addressed extensional tectonics over the years. Ample references to these studies can be found in the reviews and overview papers by Vendeville et al. (1987), McClay (1990), Allemand & Brun (1991), Beslier (1991), Naylor et al. (1994), McClay et al. (1996), Koyi (1997), Brun (1999), Michon & Merle (2000, 2003), Corti et al. (2003), Bahroudi

55 et al. (2003), Corti (2012), and Zwaan et al. (2019). The aim of this text is therefore not to
56 present an exhaustive review of all preceding publications, but to provide an overview of
57 analogue modelling of rift tectonics, describing the general methodology (materials and
58 scaling, set-ups and state-of the art analysis techniques), and to illustrate how these can be
59 applied for studying a variety of aspects of rifts and rifted margins. We also describe the
60 current challenges and opportunities in the field, which revolve around key topics such as
61 rheology, structural inheritance and kinematics, and hope that this work may serve as a guide
62 and inspiration for future analogue modelling studies.

63 **2. Methodology**

64
65 Before running an experiment, analogue modellers need to carefully consider factors such as
66 scaling, model materials and set-up, in order to ensure that the model simulates the chosen
67 natural tectonic setting as best as possible.

68
69 **2.1. Scaling principles**

70
71 When using analogue modelling techniques, proper scaling is necessary to guarantee (1) the
72 geometrical, (2) the kinematic and (3) the dynamic similarity between a model and its natural
73 equivalent. These similarities can be expressed by means of simple scaling equations
74 (Hubbert 1937, Ramberg 1981; Le Calvez 2002; Corti et al. 2003 and references therein).
75 Geometrical similarity implies that all dimensions (length, width, height, layer thickness, fault
76 angles) in the analogue model have the same proportions as in the natural prototype (i.e. the
77 model looks the same). Kinematic similarity signifies that the model and the natural example
78 maintain geometric similarity during their deformation without developing any temporal
79 distortions along the way (i.e. structures develop at the correct moment in time). Finally
80 dynamic similarity is established when all forces, stresses and the rheology of the materials
81 are properly translated from the natural example to the model scale (i.e. all forces maintain the
82 same relative proportions as in nature). Although it is practically impossible to incorporate all
83 detailed complexities that characterize natural geological settings into a small laboratory
84 experiment, a correct scaling of the dominant factors controlling deformation will allow the
85 scaling criteria to be fulfilled. In order to achieve this, it is important to select the proper
86 analogue materials that reproduce the behaviour of the lithosphere, and to choose an
87 experimental set-up, model dimensions, as well as a deformation rate appropriate for
88 simulating a specific tectonic setting (e.g. Bahroudi et al. 2003; Zwaan et al. 2019).

89
90
91
92 **2.2. Materials**

93
94 For modelling the brittle parts of the lithosphere, granular materials such as fine quartz sand
95 are commonly used, but other materials such as wet clay or wheat flour are also applied (e.g.
96 Schellart & Strak 2016; Reber et al. 2020). These materials, of which the rheological
97 properties can be tested with a ring-shear tester (e.g. Panien et al. 2006a) (or with a
98 rheometer in the case of wet clay, Eisenstadt & Sims 2005), have angles of internal friction
99 similar to those of materials in the brittle upper crust or upper lithospheric mantle (Panien et al.
100 2006a; Ritter et al. 2016; Klinkmüller et al. 2016), meaning that they develop similar structures
101 as their natural counterpart when subject to deformation (Fig. 1a). If necessary, it is possible
102 to mix granular materials or to wet them to adjust their properties (e.g. cohesion) (Van
103 Mechelen, 2004; Abdelmalak et al. 2016; Montanari et al. 2017). Some granular materials
104 (e.g. glass beads) have a lower angle of internal friction and can serve to represent structural
105 weaknesses such as detachment layers. Since deformation of these materials is strain rate-
106 independent, experimental deformation rates can be selected at will.

107
108 For the modelling of ductile parts of the lithosphere such as the lower crust, lower lithospheric
109 mantle or crustal décollements (e.g. shales or salt), a wide variety of viscous materials can be
110 used. Silicones are a common choice, but an overview of alternatives can be found in for
111 example Schellart & Strak (2016) and Reber et al. (2020). Often substances are mixed to
112 obtain a viscous material with the correct density and properties. These viscous materials can
113 have various rheologies, from Newtonian (linear) to power-law types, which can be tested
114 using a rheometer (e.g. Rudolf et al. 2016). Yet, they have in common that their behavior is
115 strain rate-dependent (generally strengthening with increasing strain rates, Brun 1999, 2002).
116 Therefore, it is very important to properly scale deformation rates when applying viscous
117 materials. When simulating the whole lithosphere, a low-viscosity material such as honey or
118 glucose syrup is often used to incorporate the isostatic effects of the underlying
119 (asthenospheric) mantle (Fig. 1d). It is however important to note that analogue materials do

120 generally not incorporate the effects of temperature variations in the lithosphere (e.g. melting
121 and phase changes), which poses some limitations to their application. For more information
122 on (viscous) materials, see Schellart & Strak (2016), Rudolf et al. (2016), Reber et al. (2020)
123 and references therein.

124
125

126 **2.3. Experimental set-ups and boundary conditions**

127

128 Set-ups for experimental modelling concern the method of imposing deformation on the model
129 (boundary conditions), and a first-order distinction can be made on the base of the gravity field
130 that is applied. In the past, numerous researchers have used a centrifuge set-up that allows
131 enhanced-gravity experiments (e.g. Koyi 1997 and references therein). This method, in which
132 an enhanced gravitational force (up to 200 g, Corti et al. 2003) is used to collapse the model
133 layers to create extension, allows the application of relatively stiff viscous materials while
134 respecting scaling laws, simplifying model construction. Drawbacks include the small size of
135 the model and the challenges of observing the rotating model within the closed centrifuge. Yet
136 the centrifuge method is still being used today, yielding highly relevant results in the field of rift
137 tectonics (e.g. Corti et al 2003; Agostini et al. 2009; Corti (2012); Philippon et al. 2015).

138

139 Running analogue experiments under normal gravity conditions is generally easier than the
140 centrifuge approach. Nowadays it is the most popular option, and therefore the focus of this
141 book chapter. As described by e.g. Vendeville et al. (1987), Allemand & Brun (1991) and
142 Zwaan et al. (2019) there are various set-ups to model extensional tectonics under normal
143 gravity conditions, depending on the model scale (upper crustal to lithospheric), tectonic
144 setting and inferred lithospheric strength profile (Fig. 1). An important difference between
145 these and centrifuge models is that deformation in normal gravity models is generally driven
146 by the mobile model base and/or sidewalls, i.e. by an imposed extension velocity boundary
147 condition, rather than by gravitational forces.

148

149 When studying deformation in the brittle upper parts of the lithosphere, from basin- to upper
150 crustal scale, modellers have often used a so-called plate base or conveyer base set-up, on
151 top of which the brittle model layers are sitting (Fig 1a). By moving the base plate apart with
152 the use of precise (stepper) motors, its edge forms a so-called velocity discontinuity (VD),
153 which is meant to simulate a fault in the basement that causes the brittle cover to deform
154 locally (as both are directly “coupled”, i.e. the base directly influences the brittle cover). A
155 problem with this set-up is that the “basement fault” does not allow vertical motion, which can
156 be solved with a basement block set-up (see section 3.1.1). Another basal boundary condition
157 can be applied with a compressed foam base underlying a sand layer (Fig. 1b, e.g.
158 Schlagenhauf et al. 2008; Zwaan et al. 2019). This set-up may simulate a ductile lower crust
159 directly coupled to the brittle crust. Here distributed deformation is transmitted to the brittle
160 layer as the model sidewalls move apart and the foam expands, leading to widespread
161 faulting. A rubber base can create a similar type of deformation (e.g. Bahroudi et al. 2003), but
162 may also cause strong boundary effects due to the fact that rubber, when stretched, tends to
163 contract perpendicularly with respect to the stretching direction (see e.g. Zwaan et al. 2019).

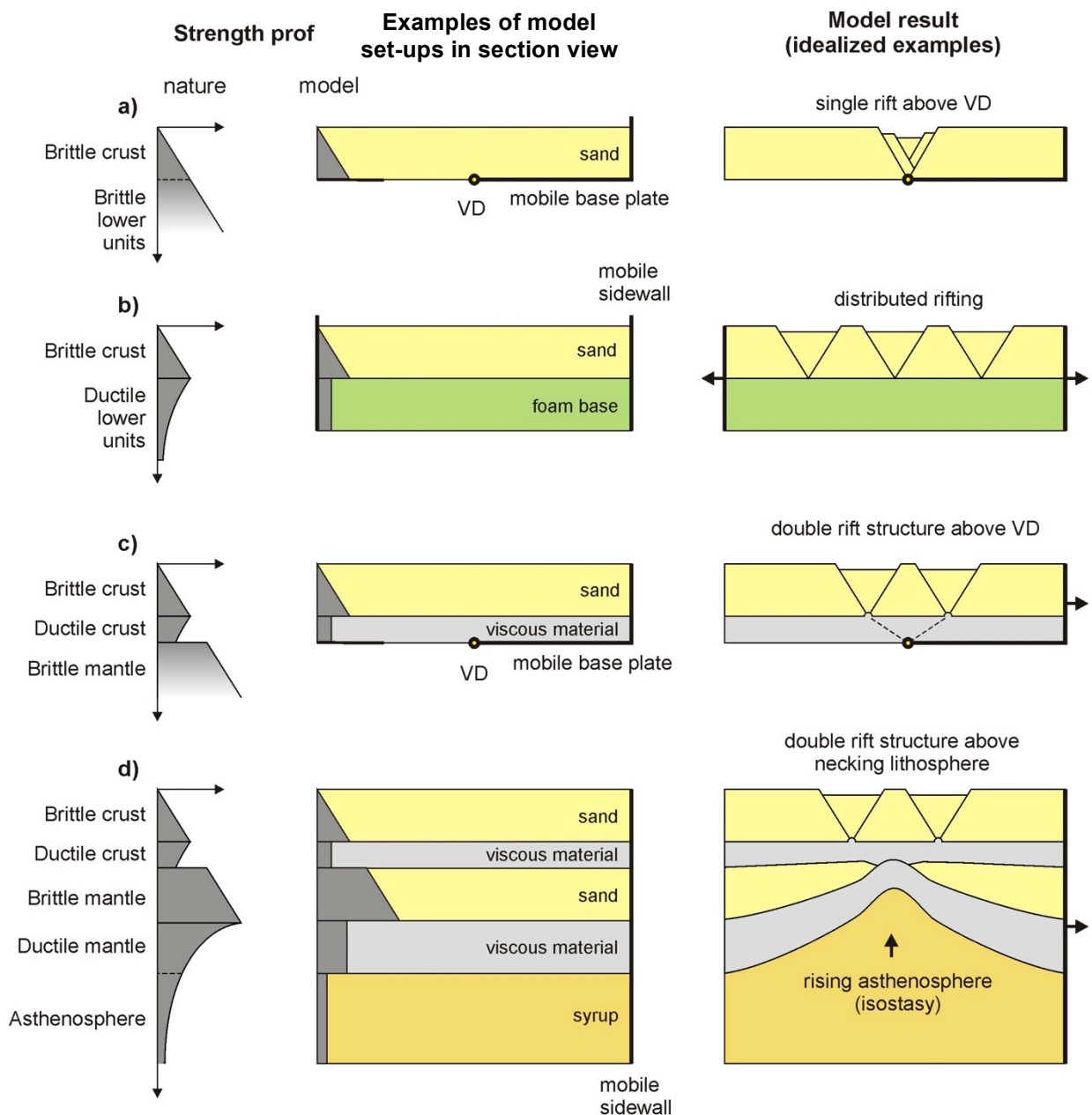
164

165 A standard model set-up for brittle-ductile settings involves a base plate system with a viscous
166 layer representing the ductile lower crust and an overlying brittle layer simulating the upper
167 crust (Fig. 1c, e.g. Tron & Brun 1991, Allemand et al. 1989; Michon & Merle 2000, 2003). Note
168 that one could also use such a layering for simulating a detachment (e.g. salt) within the brittle
169 crust (see also section 3.1.1.). Here the velocity discontinuity underlying the model materials
170 represents a fault in the brittle mantle, localizing deformation. Importantly, the viscous
171 material, if sufficiently weak, can act as a detachment layer, decoupling the brittle cover from
172 the model base, so that the latter can to a degree deform independently. Depending on
173 numerous factors, a single, double or no rift at all may develop (see also section 3.1.2).

174

175

176



177
 178 **Fig. 1.** Schematic section-view examples of normal-gravity experimental set-ups for simulating
 179 rifting at different scales, and examples of idealized results (without sedimentation). Note that
 180 slight variations in boundary conditions may have important effects on model evolution (see
 181 Figs. 4, 5). (a) Base plate set-up with brittle cover, representing a brittle-only system, develops
 182 a graben at the edge of the basal plate, where a velocity discontinuity (VD) occurs. (b) Foam
 183 base set-up, representing a brittle cover overlying a (ductile) deeper layer that evenly
 184 distributes faulting. (c) Brittle-viscous base plate model, representing a brittle-ductile crust
 185 overlying a very strong brittle mantle with a single fault (VD). Depending on various factors, a
 186 double rift may develop above the VD. (d) Four-layer Lithospheric-scale experiment on top of
 187 syrup representing the asthenosphere, allowing isostatic compensation. Deformation is
 188 induced by moving the model sidewall. Compare with (c). Modified after Allemand & Brun
 189 (1991), Brun (1999, 2002) and Zwaan et al. (2019).

190
 191
 192 Finally, when simulating rifting of the entire lithosphere, modellers need to include the mantle
 193 lithosphere and the underlying asthenosphere, which allows for isostatic compensation (Fig.
 194 1d). In this case, four-layer models representing the brittle and viscous parts of the lithosphere
 195 are mostly used, although modellers have also worked with three-layer systems (e.g.
 196 Allemand et al. 1989). A very weak viscous layer such as honey or glucose syrup is used as

197 an analogue for the asthenosphere. By moving the sidewalls apart, the layers are stretched.
198 Also in these models, numerous factors, especially the coupling between the various layers
199 (itself a function of viscosity and strain rate), may affect the style of rifting (see section 3.1.3).

200
201 When applying analogue models, their layering translates to a strength profile that should be
202 similar between model and nature (e.g. Zwaan et al. 2019; Fig. 1). Whereas the brittle part of
203 the profiles are mostly matched fairly well, the depth-dependent strength decrease in the
204 ductile domain often remains an approximation since the effects of increased heating and
205 pressure are challenging to incorporate. Also, various other lithospheric strength profiles may
206 occur in nature, which can be replicated with different materials and layer thicknesses.

207
208 Furthermore, it may be necessary to control where deformation occurs in a model to ensure
209 reproducibility, or to simulate pre-existing structures that reactivate. In the case of direct
210 coupling, faulting will be directly affected by the model base (1a, b). Yet when viscous layers
211 decouple the model components, modellers can for instance apply “seeds” (rods of viscous
212 material) at the base of the brittle cover to weaken it locally (e.g. Le Calvez & Vendeville,
213 2002, Zwaan et al. 2016; Molnar et al. 2019) or create pre-cut faults within the brittle layer
214 (e.g. McClay et al. 2002; Bellahsen & Daniel 2005), to localize deformation. On a lithospheric
215 scale, modellers have also used weak zones within the upper mantle analogue to focus
216 deformation (Molnar et al. 2017).

217
218 The examples of model set-ups in Fig. 1 are shown in section view, and analogue models
219 have often been depicted and analysed as such. This is permissible if the section is parallel to
220 the deformation direction, and if no variations along the rift axis are included, so that
221 deformation can be assumed to have occurred in plane. Yet it is important to emphasize that
222 any analogue model experiment is 3D, and that numerous models incorporate processes that
223 act in the third dimension. For these experiments, analysis cannot be limited to a single 2D
224 section.

225

226

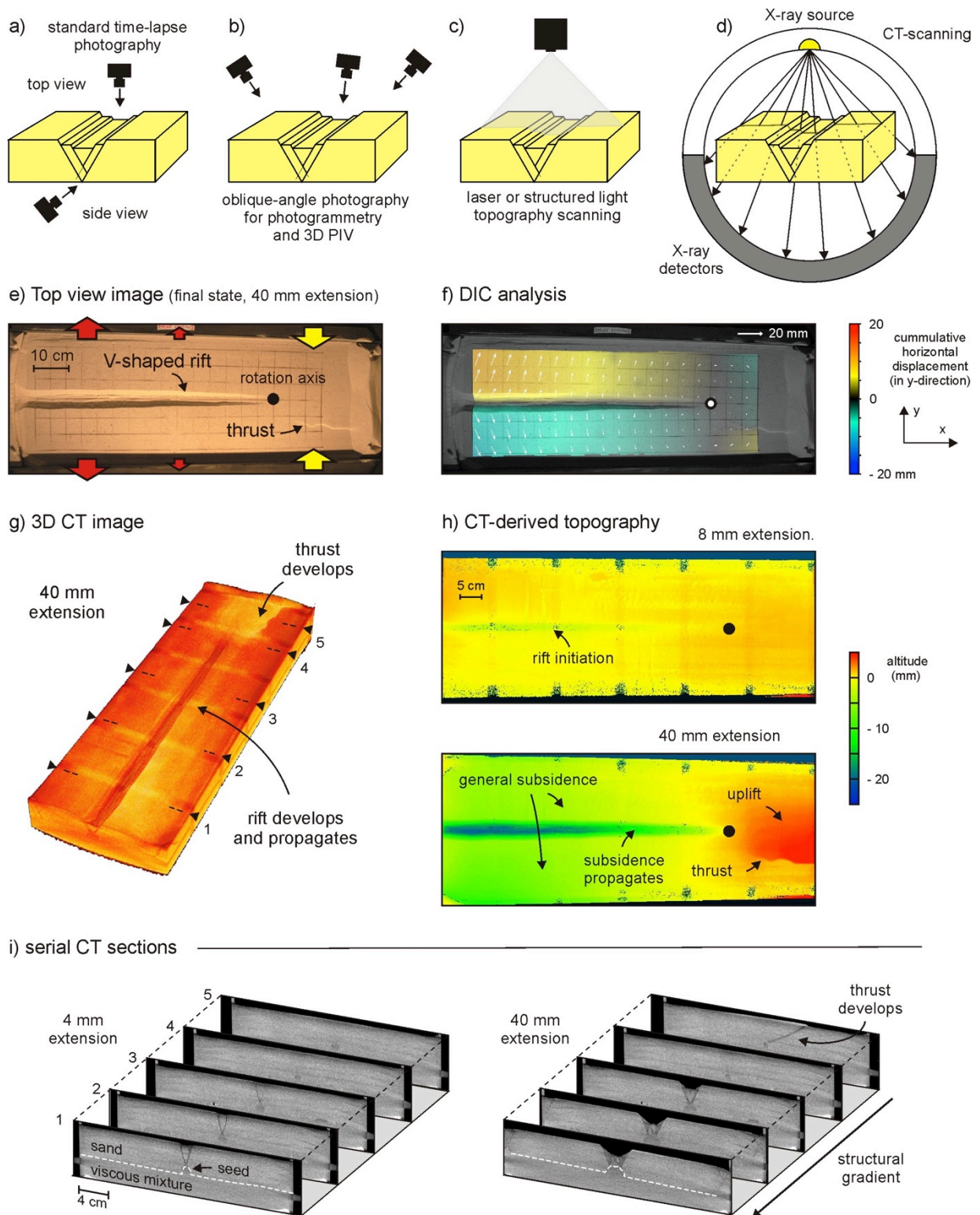
227 **2.4. Model analysis techniques**

228

229 Researchers have been using increasingly sophisticated techniques to capture deformation in
230 their analogue experiments. The most basic option, used since the early days of modelling, is
231 photography (Fig 2a). Top view images are a great help for visualizing model evolution and
232 are part of the standard toolkit of any analogue model laboratory. Automated time-lapse
233 photography allows modellers to follow deformation in great detail. Moreover, if the model set-
234 up includes a transparent sidewall, side view photographs provide valuable insights in how the
235 model is deforming internally, although researchers must be aware of potential boundary
236 effects due to sidewall friction. A very common alternative is to make cross-sections of the
237 experiment. Yet in order to do so, the model must be stabilized (e.g. wetted, frozen, or
238 impregnated with gelatine) and physically cut. Although several labs have elevated such
239 techniques to an art-form, cutting very fine sections, of which the photographs can be
240 imported in structural interpretation software for detailed analysis (e.g., Wu et al. 2009;
241 Withjack et al. 2017; Dooley & Hudec 2020), it means that the model must be destroyed and
242 the resulting information only represents the final model state. Still such sections provide
243 instructive insights in model structures and form the basis of several figures presented in this
244 book chapter.

245

246 Researchers commonly add surface markers (e.g. a grid) or differently colored sand layers to
247 visualize deformation in map view and side view/cross-section photographs, allowing a semi-
248 quantitative assessment of deformation (Fig. 2e). More precise analysis of such data can be
249 achieved by means of particle image velocimetry (PIV) or digital image correlation (DIC) of
250 time-lapse series (e.g. Adam et al., 2005; Boutelier et al. 2019). These techniques compare
251 photographs from different time steps tracing and displaying 2D displacement (Fig. 2f). The
252 now fully quantified 2D displacement patterns furthermore allow detailed strain analysis (e.g.
253 e.g. Boutelier & Oncken 2011).



254
 255
 256 **Fig. 2.** Experimental monitoring techniques. (a) Top- and side-view photography, for 2D
 257 PIV/DIC analysis. (b) Oblique-angle photography for topographic and 3D PIV/DIC analysis. (c)
 258 Surface scanning for topographic evolution monitoring. (d) X-Ray CT-scanning allowing non-
 259 destructive inspection of internal model evolution, as well as internal PIV/DIC and DVC
 260 analysis. (e-i) Application of various analysis techniques on a rotational extension experiment
 261 from Zwaan et al. (2020). (e) Top view of final model state. (f) Quantification of cumulative
 262 horizontal displacement through DIC analysis. (g) 3D CT imagery of the final deformation
 263 stage. (h) CT-derived topography maps. (i) Serial CT sections of internal structures over time,
 264 showing the structural gradient in the early and final stages of the model run. Note the
 265 structural weakness (seed) that localizes deformation. Section locations are indicated in (g).

266
267 Nevertheless these results represent only 2D insights, whereas the processes in models and
268 in nature are three-dimensional. By using stereoscopic camera configurations or
269 laser/structured light scanners, it is possible to capture 3D surface deformation (e.g.
270 Donnadieu et al. 2003; Michon & Sokoutis 2005; Schlagenhauf et al. 2008; Nestola et al.
271 2015). Photogrammetry software can reconstruct detailed digital elevation models that allow
272 researchers to quantify vertical displacement. Yet more sophisticated is 3D surface analyses
273 by means of PIV software. Similar to normal photogrammetry software, this 3D PIV technique
274 reconstructs the surface of the model, and goes a step further than 2D PIV methods by tracing
275 vertical displacements as well (e.g. Adam et al. 2005; Molnar et al. 2017, Ge et al. 2019). As a
276 result, this technique allows a unique and fully quantified 3D analysis of surface deformation.
277

278 However, these techniques do not provide a complete insight into internal model deformation.
279 This can so far only be achieved by means of X-ray CT-scanning, during which the model is
280 not physically disturbed (e.g. Naylor et al. 1994; Colletta et al. 1991; Schreurs et al. 2003), in
281 contrast to cutting it to obtain cross-sections. The method has some limitations in that both the
282 set-up and experimental materials need to be X-ray transparent, and the complete experiment
283 needs to fit into a (medical) CT scanner. CT-scanning however provides unrivalled potential
284 for model analysis. The model can be visualized in 3D (Fig. 2g) and it allows the extraction of
285 detailed digital topography maps, much like photogrammetry or surface scanning (Fig. 2h).
286 Furthermore the 3D CT volume allows modellers to make cross-sections in any direction they
287 desire, for every time step at which the model was scanned. This provides detailed insights
288 into internal model development (e.g. Zwaan et al. 2020, Fig. 2i), and also allows 4D analyses
289 when imported into structural interpretation software (e.g. Chauvel et al. 2018; Fedorik et al.
290 2019). Yet also these insights remain semi-quantitative. The final step is to apply PIV or DIC
291 techniques on CT data, which can be done on 2D sections from different time intervals,
292 yielding unique quantitative information (Zwaan et al. 2020), but also on successive 3D
293 volumetric CT-data sets produced at different time steps during the evolution of one particular
294 experiment. This so-called digital volume correlation (DVC) technique (Adam et al. 2013)
295 uniquely allow the tracing of displacements and the quantification of strain throughout the
296 complete model, clearly illustrating that rifting is a 3D process (e.g. Zwaan et al. 2018, Fig. 2j).
297
298
299

j) DVC analysis of orthogonal extension model with overlapping rift segments

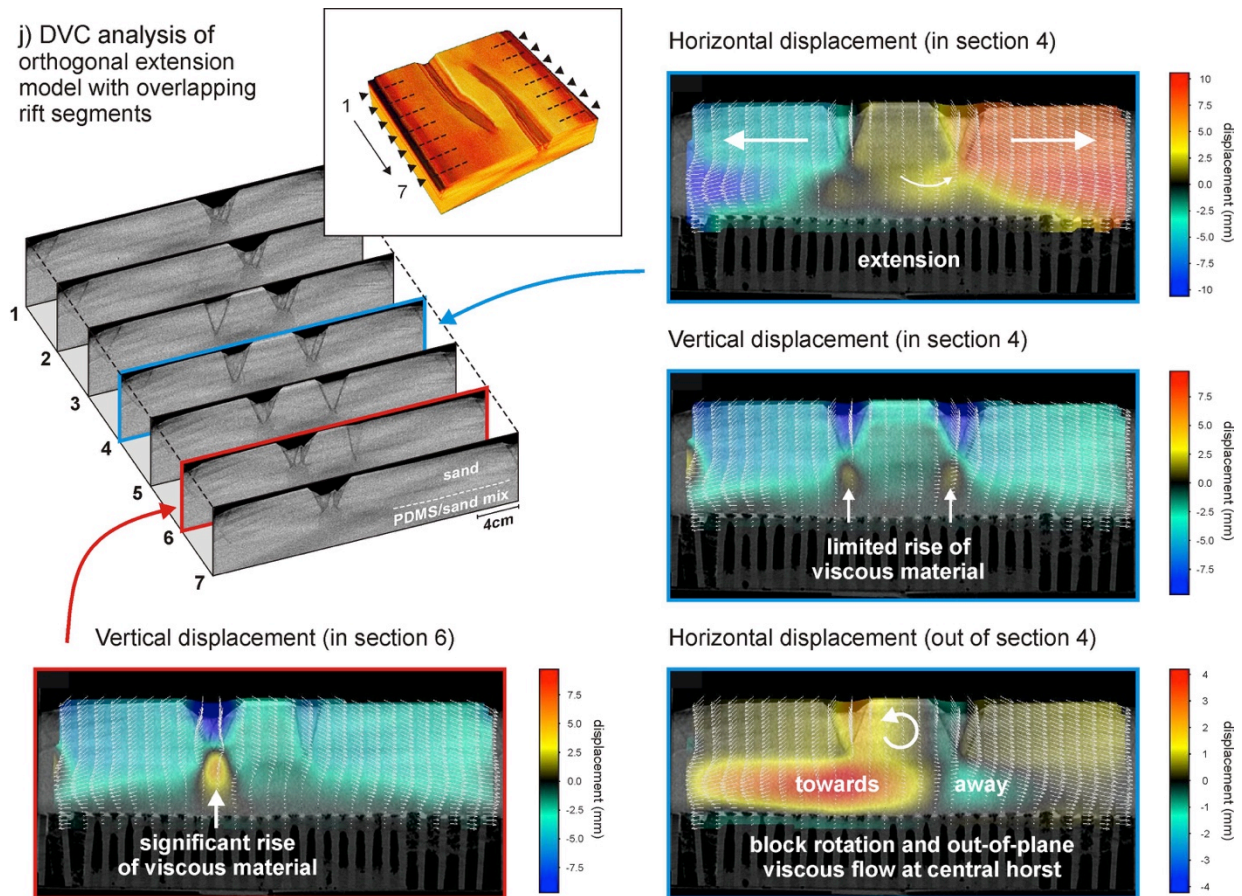


Fig. 2. (continued) (j) Example of digital volume correlation (DVC) analysis on CT data from a model with interacting rift segments under orthogonal extension, illustrating internal displacement patterns. Note the differences in vertical displacement at different places, as well as out-of-plane displacement of both brittle and viscous material, highlighting the 3D character of the system (compare vertical displacements in sections 4 and 6). Modified after Zwaan et al. (2018).

3. Model application

As described in section 2, different set-ups and materials are used to study diverse aspects of rifting on different scales. In the following, we shall provide an overview of various examples, ranging from quasi-2D models of crustal and lithospheric scale models, to experiments involving 3D rift processes such as oblique extension, rift segment interaction and rotational rifting. As emphasized in section 2.3, all analogue models are by definition 3D objects. However, rift models are often analysed in section parallel to the extension direction, which provides quasi-2D insights.

3.1. A 2D perspective on rifting

3.1.1. Normal fault development in the upper crust

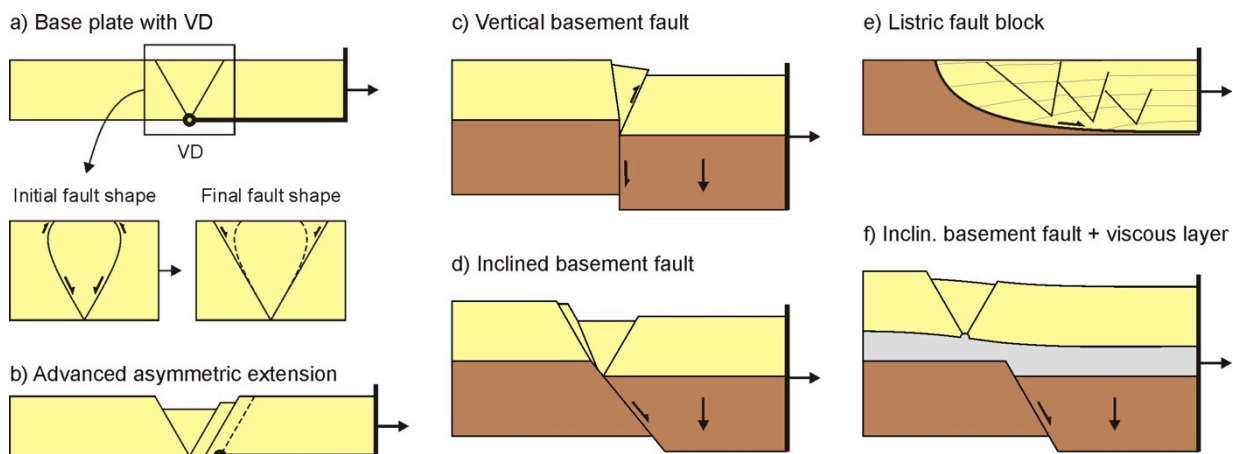
Various authors have simulated the development of normal faulting in the upper (parts of the) crust (Fig. 3). For instance the CT-scanned experiments by Panien et al. (2006a) reveal that in a brittle base plate set-up, normal faulting in the shape of a graben initiates at the basal velocity discontinuity (VD), and subsequently propagates towards the model surface (Fig 3a). Furthermore, the authors show that due to stress deflection, these initial faults may overturn towards the surface, becoming reverse faults in the upper few mm of the model (Fig. 3a).

331 Later on, the lower part of the normal fault is reactivated and continues upward in the footwall
 332 with the initial subvertical and reverse segments being abandoned. Such features are also
 333 found in nature (Trippanera et al. 2014), most spectacularly at the rims of collapsed calderas
 334 (Martí et al. 2008). When extension is asymmetric, the resulting fault pattern will also be
 335 asymmetric, as new faults develop above the edge of the moving base plate (e.g. McClay
 336 1990; Beslier 1991; Allemand & Brun 1991, Fig. 3b).

337
 338 Other researchers have studied the effects of basement block subsidence on fault
 339 development in the sedimentary cover. Naylor et al. (1994) show how vertical basement faults
 340 can cause reverse faulting in the overburden (Fig. 3c), in a process similar to the reverse
 341 faults described by Panien et al. (2006a) (Fig. 3a). By contrast, models with low-angle
 342 basement faults create a graben structure above the fault (Naylor et al. 1994; Holland et al.
 343 2006) (Fig. 3d). Furthermore, if the basement fault is listric, a roll-over structure forms, and if
 344 syn-rift sedimentation is applied by stepwise filling up the generated accommodation space, a
 345 series of small grabens will develop in the accumulating hanging wall strata (e.g. McClay
 346 1990, Fig. 3e).

347
 348 Moreover, adding a layer of relatively weak viscous material to simulate salt or shale
 349 detachments can decouple the brittle cover from the model basement (e.g. Vendeville et al.
 350 1995; Dooley et al. 2003, Fig. 3f). As a result, flexure can develop as the viscous material
 351 flows, and normal faulting in the brittle layer can be displaced sideways with respect to the
 352 underlying basement fault (Fig. 3f).

353
 354



355
 356
 357 **Fig. 3.** Schematic examples of upper crustal scale models to study normal faulting. (a) Base
 358 plate creating a graben in the brittle material above the velocity discontinuity (VD) at its plate
 359 edge (top). Initial fault may be curved, leading to local reverse kinematics (bottom left). Later
 360 on, full normal faulting is established (bottom right). (b) When extension is asymmetric, an
 361 asymmetric graben will form after advanced deformation. Modified after Allemand et al.
 362 (1989), Panien et al. (2006a). (c) Vertical (high angle) basement fault causing reverse faulting
 363 in the brittle cover. Modified after Naylor et al. (1994). (d) Inclined (low angle) basement fault
 364 inducing normal faulting and graben formation in brittle cover. Modified after Naylor et al.
 365 (1994). (e) Listric fault model developing a roll-over anticline with internal grabens. Modified
 366 after McClay (1990). (f) Effect of a decoupling viscous layer on faulting in the brittle cover
 367 above a basement fault. Compare with (d). Modified after Dooley et al. (2003).

368
 369
 370
 371
 372
 373
 374

375 **3.1.2. Brittle-viscous crustal scale models**

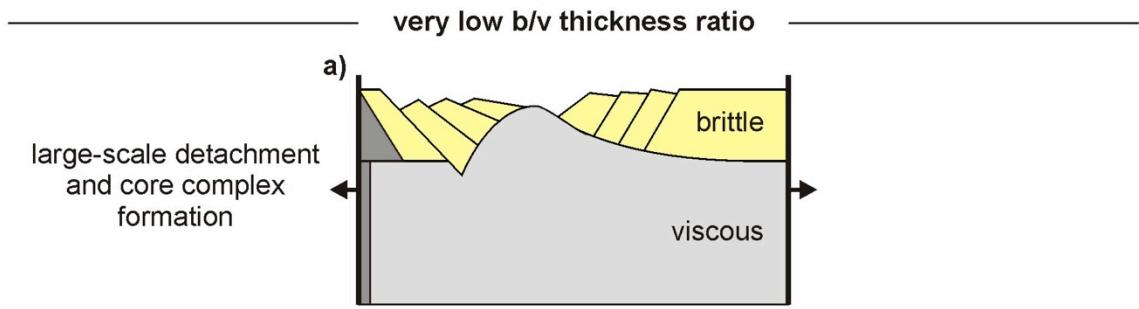
376
377 When zooming out to full-crustal scale, applying brittle-viscous layers representing the entire
378 brittle-ductile crust, researchers have found various influences of lithospheric strength (i.e.
379 layer thicknesses and extension rates) as well as model boundary conditions on the mode of
380 rifting (Brun 1999; Corti et al. 2003; Zwaan et al. 2019 and references therein). A very thick
381 viscous layer, representing for instance the effect of crustal thickening and radioactive heating
382 in an orogen, creates a very weak crust (Fig. 4a). As a result, the brittle cover is very much
383 decoupled from the model base, which induces detachment faulting and the formation of
384 exhumation structures analogue to metamorphic core complexes (Brun et al. 1994, Fig. 4a).

385
386 By contrast, a thinner viscous layer (low brittle-to-viscous thickness ratio), representing a
387 colder crust, leads to localized rifting when extension rates are low (Fig. 4b). However, when
388 applying high extension rates, the viscous layer is stronger and coupling between the viscous
389 and brittle layers is enhanced so that they start deforming together, causing distributed
390 faulting (“wide rift mode”, Brun 1999) (Fig. 4c).

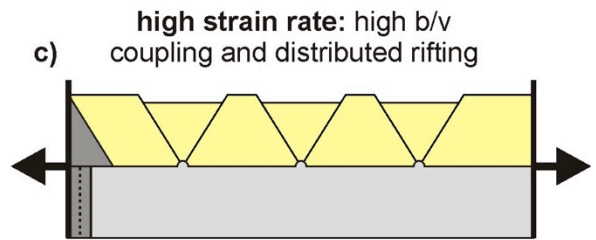
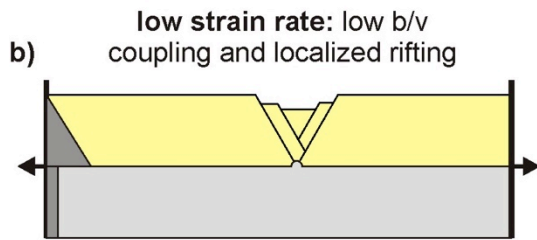
391
392 When the viscous layer is even thinner as may be the case in an older, cold crust, the basal
393 boundary condition starts to affect the style of rifting (Fig 4d-f). This boundary condition was
394 not particularly important in the previous cases due to a high degree of decoupling between
395 model base and brittle layer (Fig. 4a-c). However, increased coupling between the base and
396 brittle cover rifting causes the materials to deform in a similar way as in the models without a
397 viscous layer (Figs 1a, b, 3a-d, 4d-f). A foam base (simulating a ductile/weak mantle) causes
398 distributed extension throughout the brittle cover (Fig. 4d), whereas a plate base (simulating a
399 strong/brittle mantle) causes more localized deformation (Zwaan et al. 2019, Fig. 4e). Whether
400 a single or double rift develops in the latter depends on the extension rate (Michon & Merle
401 2000).

402
403 Further influences on the evolution of brittle-viscous rift systems are caused by the application
404 of asymmetric extension and sedimentation. Simply put, symmetric rifting will lead to
405 symmetric rift structures, whereas asymmetric rifting, if coupling between the base and brittle
406 cover is significant enough, may cause the rift to focus on the moving plate, away from the
407 basal velocity discontinuity (Allemand & Brun 1991, Fig. 4f). Moreover, syn-rift sedimentation
408 can not only prevent the brittle layer from breaking up so that deformation remains focused
409 along a few large normal faults (Fig. 4h), but the weight of the sediment infill also prevents
410 viscous material from rising below an otherwise thinned rift wedge (Zwaan et al. 2018, Fig. 4g,
411 h). Such flow of viscous material below the rift basin can be clearly visualized by means of
412 displacement analysis on CT data (Zwaan et al. 2018, 2020, Fig. 2j).

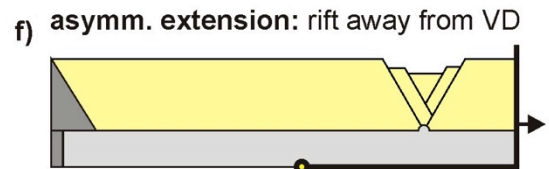
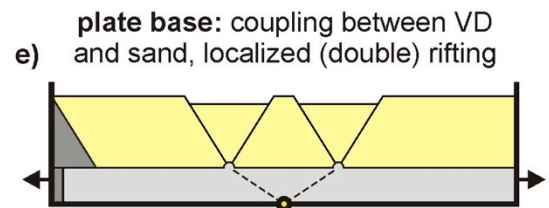
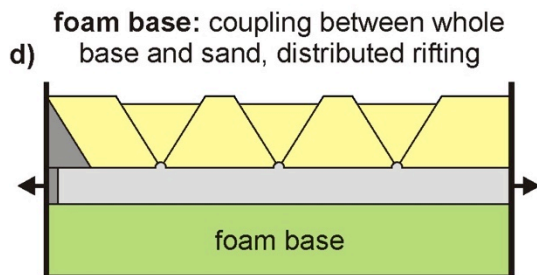
413
414



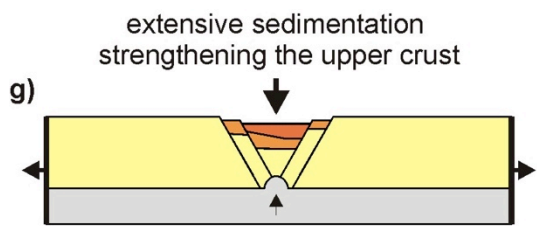
low thickness ratio (= ca. 1)



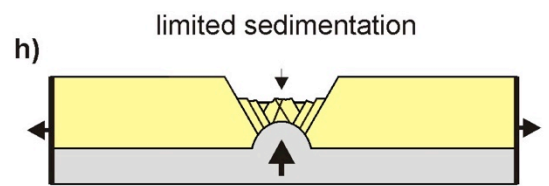
high b/v thickness ratio



syn-rift sedimentation



important sedimentary loading,
limited upwelling of viscous material



no sedimentary loading,
strong upwelling of viscous material

415
416
417

418 **Fig. 4.** Schematic examples of parameters affecting brittle-viscous experiments. (a) Very low
419 brittle-to-viscous (b/v) thickness ratios (i.e. very low strength) decouple the brittle layer from
420 the base, leading to core complex formation. Modified after Brun et al. (1994). (b-c) Low b/v
421 thickness ratios still decouple the brittle layer from the base, yet high strain rates cause
422 distributed faulting (wide rifting mode), whereas low strain rates localize deformation (narrow
423 rifting mode). Modified after Brun (1999) and Zwaan et al. (2019). (d-f) A thin viscous layer
424 leads to coupling between base and brittle cover. For foam base set-ups, the foam's
425 distributed deformation transfers to the brittle cover, which develops widespread faulting. A
426 base plate set-up causes localized deformation above the velocity discontinuity (VD), yet
427 depending on strain rate a single or double rift may develop. Modified after Michon & Merle
428 (2000, 2003). Furthermore, asymmetric extension may (in some cases) deflect deformation
429 away from the VD (Allemand et al. 1989). (g-h) Effects of sedimentation on rift development.
430 Sedimentary infill causes strengthening of the brittle layer, focusing fault activity along a few
431 faults, and suppressing upwelling of viscous material. Absence of sedimentation causes the
432 rift wedge to split along numerous faults while the viscous layer rises. Modified after Zwaan et
433 al. (2018). Note that the dark grey on the left of the images represents the strength profile.

434
435

436 **3.1.3. Lithospheric scale models**

437

438 For crustal-scale models, it is not always necessary to incorporate the (isostatic) effects of the
439 deeper mantle layers. But as plate tectonics involves the entire lithosphere, which is in
440 isostatic equilibrium with the asthenosphere, both are included in various large-scale model
441 studies of rifting (e.g. Allemand et al. 1989; Brun & Beslier 1996; Nestola et al. 2015; Molnar
442 et al. 2017; Beniest et al. 2018). These experiments show that the presence of a competent
443 upper mantle layer is of great importance (Corti et al. 2003). When such a layer is absent, the
444 strength of the lithosphere is dominated by the upper crust, leading to localized rifting (Fig. 5a,
445 similar to Fig. 4b). When present, this competent upper mantle controls the strength of the
446 lithosphere and its rupture creates either a single or double rift in the brittle upper crustal layer
447 (Fig. 5b, c, compare with Figs. 1c, 4e).

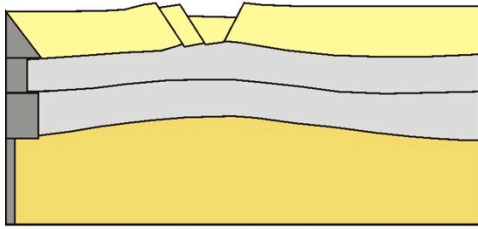
448

449 In such four-layer lithospheric models, (de)coupling between brittle and viscous layers is
450 highly important. When coupling is low, either due to low strain rates or low viscosities in the
451 ductile domain (Brun 1999; 2002), deformation is localized in both the brittle mantle and crust,
452 which may represent natural rift settings like in the Upper Rhine Graben (Beslier 1991, Brun
453 1999, Fig. 5c). By contrast, enhanced (intermediate) brittle-viscous coupling causes a more
454 distributed style of rifting and may lead to exhumation of the model mantle as observed in
455 nature along the Atlantic margin of Iberia (Fig. 5d, Brun & Beslier 1996). On the other hand,
456 extension of models with high coupling between its viscous and brittle components may cause
457 widespread deformation (Beslier 1991, Fig. 5e, compare with Fig. 4c and d).

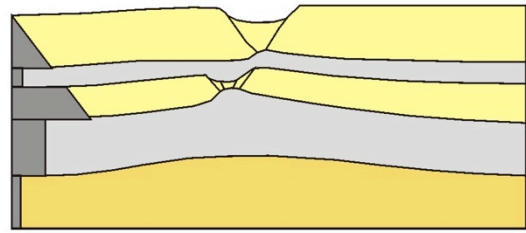
458

459 The models in Fig. 5 do however not consider structural inheritance. Other researchers have
460 included crustal and mantle weaknesses to localize deformation (e.g. Agostini et al. 2009).
461 Beniest et al. (2018) have studied lateral strength variations and show how rifting
462 predominantly localizes in the weaker part of the lithosphere (i.e. away from competent areas
463 such as cratons). Corti et al. (2003) include low-viscosity patches to represent melts and
464 provide a schematic overview of the relative relations between various parameters and rift
465 styles (their Fig. 36). But although these models yield valuable insights in rift processes,
466 including mantle exhumation (Brun & Beslier 1996, Fig. 5d), analogue models are limited to
467 the continental rifting phase, given that commonly applied materials do not allow the creation
468 of new oceanic lithosphere.

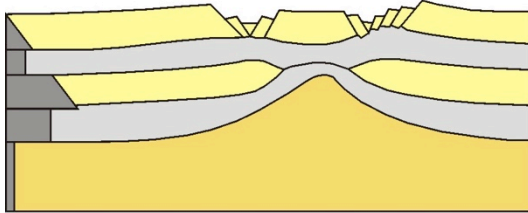
a) three layers: B/V/V



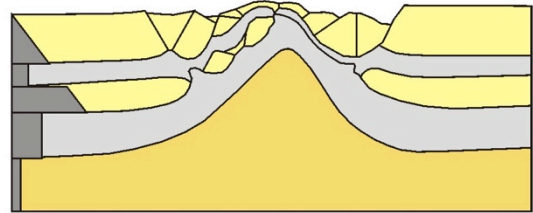
c) four layers: low B/V coupling



b) four layers: B/V/B/V



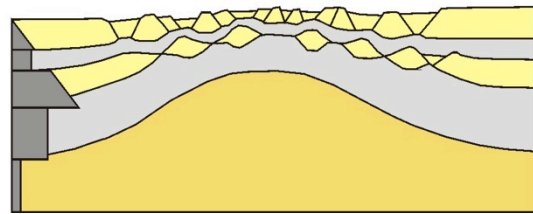
d) four layers: intermediate B/V coupling



5 cm

- brittle materials (crust and mantle)
- viscous materials (crust and mantle)
- syrup/honey (asthenosphere)

e) four layers: high B/V coupling

470
471

472 **Fig. 5.** Schematic examples of lithospheric-scale rift model results as a function of (a, b)
473 lithospheric layering (three vs. four layers) and (c-e) degree of coupling between the brittle
474 and viscous materials (B/V coupling) in four-layer models. B: brittle, V: viscous (ductile).
475 Modified after Allemand et al. (1989), Beslier (1991), Brun & Beslier (1996) and Brun (2002).

476
477

478 3.2. Exploring 3D rift processes

479

480 Although many studies have approached lithospheric extension as a 2D phenomenon and
481 analysed it accordingly, various authors have explored the third dimension as well. Their
482 results show the importance of understanding the 3D aspects of rift processes, resulting from
483 e.g., oblique extension, the interaction between individual rift segments, rotational rifting or rift
484 propagation.

485

486 3.2.1. Oblique extension

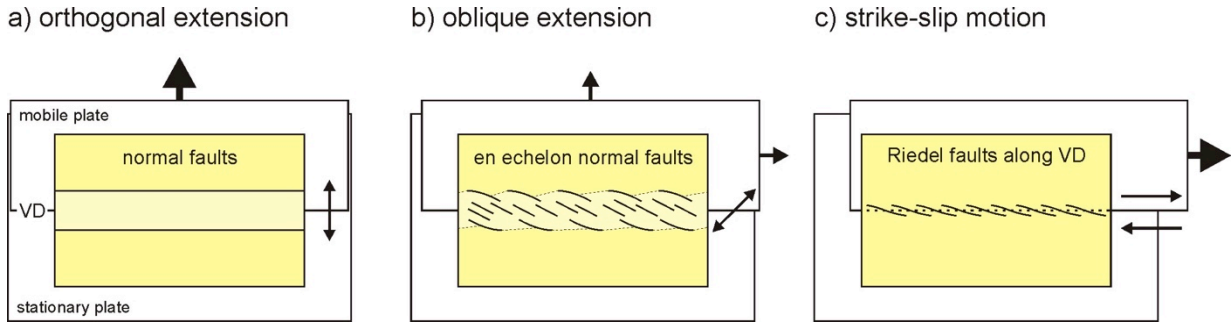
487

488 Most extensional systems experience some form of oblique extension during their life-time
489 (Brune et al. 2018) and researchers have extensively used analogue models in order to
490 understand the significance of this parameter, (e.g. Withjack & Jamison 1986; Tron & Brun
491 1991; McClay & White 1995; Clifton et al. 2000; Agostini et al. 2009; Autin et al. 2010, 2013).
492 These studies show that under orthogonal extension settings, large normal faults strike
493 perpendicularly to the extension direction and thus parallel to the rift axis (Fig. 6a). Yet when
494 extension is oblique, the faults strike at an angle to the rift axis (although not perpendicular to
495 the extension direction, see Withjack & Jamison 1986), and the resulting rift zone is bordered
496 by en echelon boundary faults (Fig. 6b). Although the boundary faults are oriented obliquely to
497 the rift axis, their kinematics remain dominantly normal (Philippon et al. 2015). With increasing
498 obliquity towards the strike-slip domain, however, normal faults will give way to strike-slip

499 faults. Typical for such models is the development of initial Riedel shears above the rift axis,
500 which subsequently link up to form a continuous strike-slip fault (e.g. Naylor et al. 1986;
501 Dooley & Schreurs 2012 and references therein, Fig. 6c).

502
503 Furthermore, Keep & McClay (1997), Bonini et al. (1997) and others explore the effects of
504 multiphase oblique extension and show how structures formed during the initial phases are
505 often reactivated to dominate subsequent extension phases. However, the reactivation of pre-
506 existing structural weaknesses in the crust or mantle under (oblique) extension only localizes
507 deformation when oriented favorably to the regional (oblique) extension direction (Zwaan &
508 Schreurs 2017; Molnar et al. 2019). On a lithospheric scale, Autin et al. (2010) describe how
509 their models suggest that oblique extension may protract break-up.

510
511



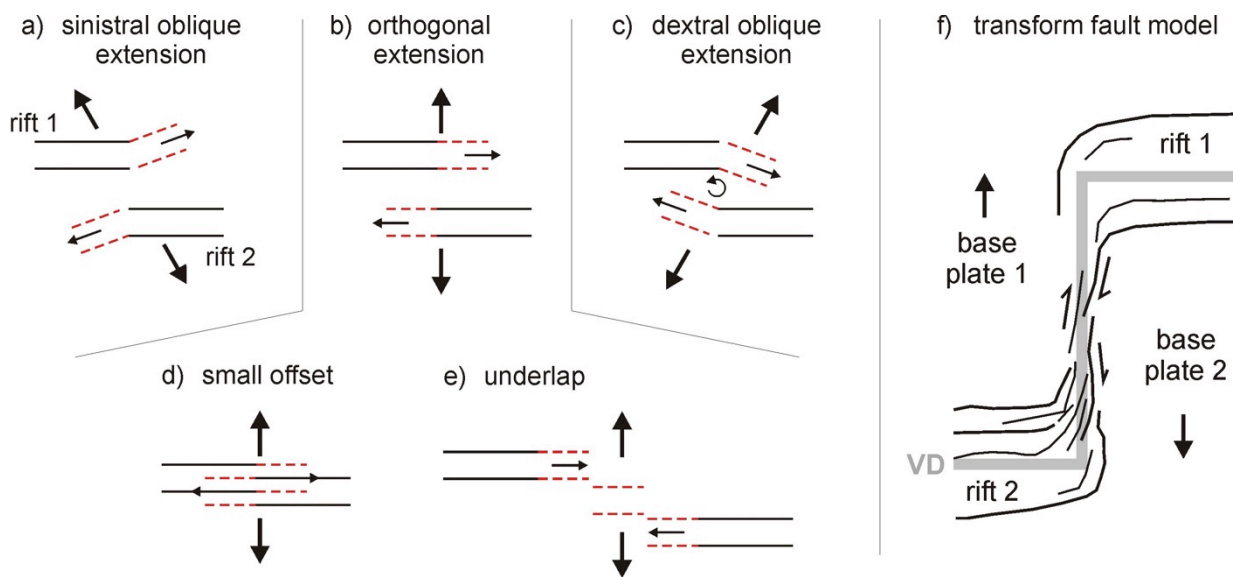
512
513
514 **Fig. 6.** Schematic map view examples of fault patterns related to different extension directions
515 as observed in experiments. (a) orthogonal extension leads to long, velocity discontinuity
516 (VD)-parallel normal faults. (b) when extension is oblique, en echelon normal faults develop
517 along the VD, but their strike is not perfectly perpendicular to the extension direction (Withjack
518 & Jamison 1986). (c) Under strike-slip conditions, a series of Riedel shears appear above the
519 VD, which in later stages connects to form a continuous strike-slip fault. Modified after Tron &
520 Brun (1991). Note that in the set-ups shown in (a) and (b) the diverging base plates are
521 generally connected by a rubber sheet or partly overlain by a patch of viscous material.

522
523
524
525

526 **3.2.2. Rift segment interaction**

527
 528 When the lithosphere is stretched, deformation often localizes along pre-existing structural
 529 weaknesses to form individual rift segments. In order to develop into a full-scale rift system,
 530 these segments need to interact, propagate and connect. Analogue studies show that such rift
 531 interaction structures are affected by the horizontal distance (offset), the amount of underlap
 532 or overlap between rift segments, and the presence of secondary pre-existing weaknesses
 533 linking the segments and oblique extension (e.g. Acocella et al. 1999; Le Calvez & Vendeville
 534 2002; Tentler 2003a, b; Molnar et al. 2019). The effect of the latter is well visible if the offset
 535 between rift segments is sufficiently large (Fig. 7a-c). Since normal faults tend to develop at
 536 high angles to the regional extension direction (see section 3.2.1), rift segments propagate
 537 either away from, parallel to, or toward each other. In the latter case, the central block may
 538 become isolated (rift pass structure) and can start rotating due to the interaction between the
 539 overlapping rift axes (Zwaan et al. 2018, Figs. 7c, 2j), a process currently observed at the
 540 Victoria Plate in the East African Rift (Glerum et al. 2020). In situations with small offsets,
 541 these effects will not occur as the rift segments readily grow into each other (Fig. 7d).
 542 Furthermore, when the rift segments underlap, a series of minor en echelon grabens may
 543 develop (e.g. Tentler 2003a, b, Fig. 7e). Some models show that secondary pre-existing
 544 weaknesses may help to connect rift segments, but only if these are oriented favorably to the
 545 extension direction; if they are aligned (sub-)parallel to the extension direction they will not
 546 activate (Zwaan & Schreurs 2017; Molnar et al. 2019). Yet when applying strongly controlling
 547 basal boundary conditions with a plate base set-up, it is possible to force the development of
 548 transform fault-like structures along the edge of the plate, even if this velocity discontinuity is
 549 aligned with the extension direction (e.g. Acocella et al. 1999; Dauteuil et al. 2002, Fig. 7f).

550
 551
 552



553
 554

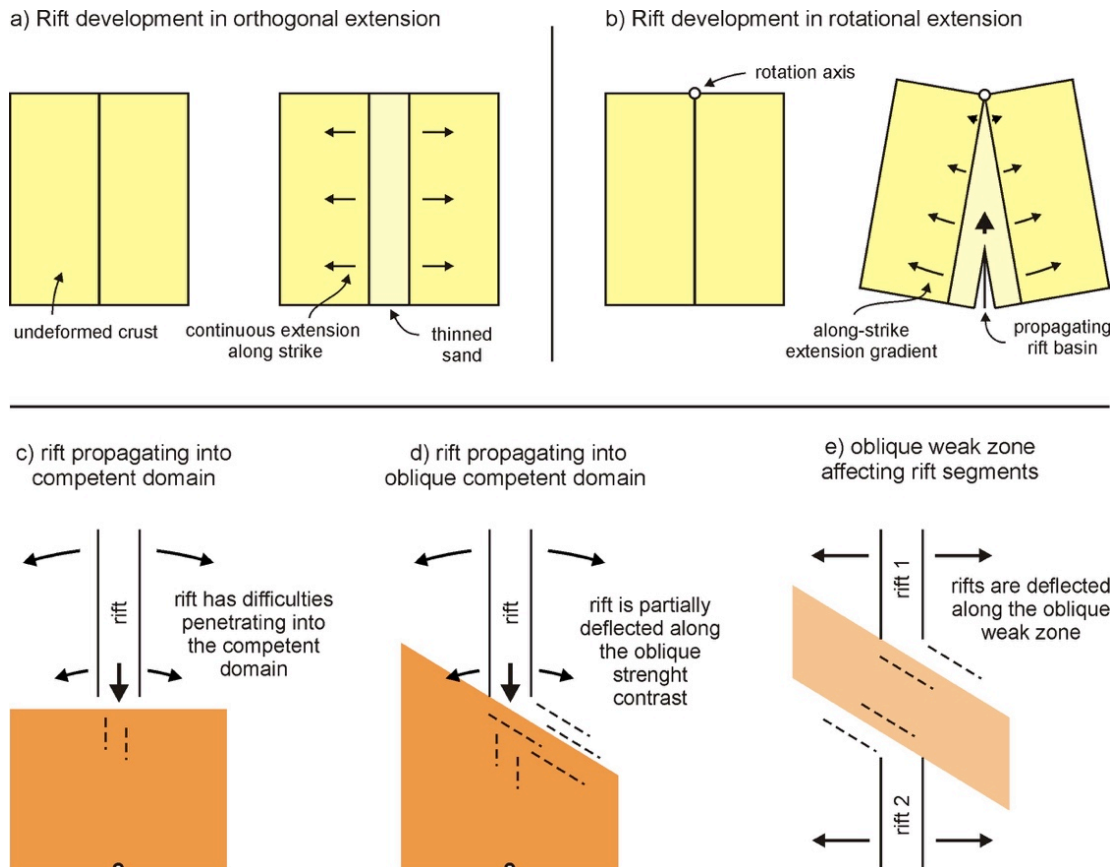
555 **Fig. 7.** Schematic examples of modelled rift interaction between right-stepping rift segments,
 556 depending on extension direction. Since the strike of new normal faulting tends to be at high
 557 angles with respect to the extension direction (Withjack & Jamison 1986), (a) sinistral oblique
 558 extension causes the rifts to diverge, (b) orthogonal extension has the rifts grow in a parallel
 559 fashion and (c) dextral oblique extension lets the rifts grow together. The block in between the
 560 rifts in (c) can start rotating and even form a continental sliver or microcontinent. Note that the
 561 relations between rift development and extension direction as shown in this figure are
 562 opposite when the rift segments are arranged in a left-stepping fashion. (d) Rifts directly grow
 563 into each other when their offset is small. (e) Rifts may create en echelon interaction zones
 564 when underlap and offset are sufficiently large. (f) Transform fault modelled by a plate base
 565 set-up. VD: velocity discontinuity. Modified after Dauteuil et al (2002); Tentler (2003a, b),
 566 Zwaan et al. (2016) and Zwaan & Schreurs (2017).

567
 568
 569
 570
 571
 572
 573
 574
 575
 576
 577
 578
 579
 580
 581
 582
 583
 584
 585
 586
 587
 588
 589
 590
 591
 592
 593
 594
 595
 596

3.2.3. Rotational rifting and rift propagation

When running rifting experiments, modellers generally apply constant extension rates along the length of their models (Figs. 6, 8a). Yet plate tectonics on a globe demands rotational motion about an Euler pole, whereas various cases of smaller-scale plate rotations are recorded around the world (Zwaan et al. 2020, Fig. 8a). A few analogue modellers have explored the implications of rotational boundary conditions (e.g. Souriot & Brun 1992; Benes & Scott 1996; Sun et al. 2009; Molnar et al. 2017). These models invariably show that rift development in rotational settings causes structural gradients, rift propagation and the formation of V-shaped basins, whereas constant along-strike extension rates lead to cylindrical structures (Figs. 2e-j, 6, 8). In addition, pressure gradients in such models cause not only cross-strike displacements (Fig. 2j), but also along-strike flow of viscous material, highlighting the importance of a 3D mindset when studying rifting processes (Zwaan et al. 2018, 2020). DVC analysis of CT data clearly shows the interaction between deep-seated viscous deformation and surface deformation (Fig. 2j).

The models depicted in Fig. 8a and b concern a homogeneous layer cake. Molnar et al. (2017, 2018, 2019) describe how structural weaknesses of various types and orientations can (partially) reorient propagating rift systems. Benes & Scott (1996) test how such propagating rifts interact when encountering a competent domain, and describe how the rift has trouble penetrating the latter (Fig. 8c). When the rheological contrast is perpendicular to the extension direction, the well-defined propagating rift spreads out over various faults. Yet if the rheological contrast is obliquely oriented, part of the deformation is deflected along it (Fig. 8d). A similar result is obtained by Brune et al. (2017), who use both analogue and numerical models to study how an oblique weak zone affects rift interaction, although the authors use constant-along strike strain rates (Fig. 8e).



597
 598

599
600 **Fig. 8.** Schematic examples of rift development and propagation under different boundary
601 conditions. (a) Orthogonal extension causes synchronous rift development along its axis.
602 Oblique extension boundary conditions produce similar results (Fig. 6). (b) Rotational rifting,
603 inducing a strain rate and structural gradient, as well as rift propagation toward the rotation
604 pole. Compare with Fig. 2e-i. (c) Rift propagating into a competent domain orthogonal to the
605 rift axes. (d) Rift propagating into a competent domain oblique to the rift axes. (e) Rift
606 deflection along a zone of different rheological competence. Modified after Vink (1980) and
607 Martin (1984), Benes & Scott (1996) and Brune et al. (2017).

608
609
610 **4. Summary, challenges and future opportunities**

611
612 In the above pages, we have described how analogue modelling techniques have been used
613 to study a wide variety of aspects associated with rifting processes, from normal fault
614 development to lithospheric necking. The variety of analogue modelling methods and
615 advanced analysis techniques provides researchers with a handy and highly versatile toolkit to
616 explore factors that may affect rifting, yielding invaluable insights into the dynamic evolution
617 and associated kinematics. A key message should be that although various models have
618 focussed on the 2D aspects of rifting processes, it is evident that the third dimension needs to
619 be taken into account for a proper understanding of rifting. Analogue models thus provide
620 crucial insights, but it should be highlighted that there is still plenty of potential for
621 improvements and future applications.

622
623 Recently, Peron-Pinvidic et al. (2019) listed six main focus points for rift and passive margin
624 research efforts: rheology, structural inheritance, faulting, stratigraphy, kinematics and the
625 influence of the mantle, between which various links exist. Analogue modelling work could
626 contribute significantly to a better understanding of the role of these parameters during rifting.

627
628 (1) The influence of rheology can be addressed through analogue modelling materials as
629 researchers are constantly looking for new, adequate materials to improve model
630 performance (e.g. Schellart & Strak 2016, Reber et al. 2020). A common limitation in
631 analogue models is for instance that model material cannot undergo phase changes
632 due to thermal effects or hydration of minerals. Yet modellers have for instance used
633 materials such as paraffin wax, which melts and solidifies when changing temperature
634 (e.g. Oldenburg & Brune 1972; Brune & Ellis 1997; Katz et al. 2005), water
635 representing the asthenosphere (Chemenda et al. 2002) and gelatine to simulate
636 earthquakes (Corbi et al. 2013), although these materials often require very
637 specialized set-ups. A major breakthrough would be the development of convenient
638 analogue materials that would allow the simulation of both continental rifting until
639 break-up and the subsequent creation of oceanic lithosphere (see section 3.1.3).

640
641 (2) The role of structural inheritance (compositional, structural or thermal) can be
642 addressed in a variety of ways. Differences in lithospheric composition can be
643 simulated by using different model materials, and is strongly related to the topic of
644 rheology. Structural inheritance includes discrete weaknesses (linear seeds, pre-cut
645 faults), but it may also be possible to induce pervasive features such as a regional
646 foliation (Chattopadhyay & Chakra 2012). Furthermore, the application of multiphase
647 deformation can be of great value. Various experimental studies focus on multiphase
648 rifting (e.g. Keep & McClay 1997, Bonini et al. 1997), or inversion of rift basins (e.g.
649 Brun & Nalpas 1996, Panien et al. 2005, Mattioni et al. 2007, Cerca et al. 2010) and
650 show how pre-existing faults may, or may not, play a role during subsequent tectonic
651 phases. Vice versa, one could model another part of the Wilson cycle by simulating a
652 compressional phase that is followed by rifting.

653

- 654 (3) Analogue models are excellent for studying faulting, but how faults develop in 3D
655 space remains poorly constrained (Jackson et al. 2017). In order to get a more
656 detailed grasp of fault development during rifting, analysis techniques should be
657 optimized. Key is to fully capture model surface deformation by means of (3D) PIV/DIC
658 methods. Also detailed 3D analysis of fault populations over time by importing 3D CT
659 data in structural analysis software (e.g. Fedorik et al. 2019) will provide crucial
660 insights. Such data can also be used to create (3D) synthetic seismics, that can be
661 compared with seismic surveys from natural rift zones (Lindanger et al. 2004). Another
662 intriguing application in this line is the use of CT-scanned models to test the validity of
663 methods commonly used for tectonic restorations (Chauvin et al. 2018). The latter
664 would allow the application of numerical analysis techniques and machine learning
665 algorithms on analogue models (e.g. Corbi et al. 2019). Especially combining analogue
666 and numerical methods to tackle a specific topic calibrates modelling results and
667 strengthens their reliability (e.g. Bellahsen et al. 2003; Buitter et al. 2006; Panien et al.
668 2006b; Corti et al. 2007; Quirk et al. 2012; Zwaan et al. 2016; Brune et al. 2017;
669 Hughes et al. 2020). Also collaboration between analogue modelling laboratories
670 improves research quality and output. In order to promote such cooperation EPOS has
671 created a network of labs (Multi-scale Laboratories) allowing knowledge exchange and
672 resource sharing (<https://www.epos-ip.org/tcs/multi-scale-laboratories>).
673
- 674 (4) The development of stratigraphy in rift and passive margin settings is strongly affected
675 by faulting, but sedimentary infill, if thick enough, can itself also affect the tectonic
676 framework (Zwaan et al. 2018). The application of sedimentation processes in
677 analogue models is often rather coarse: often the basin is simply filled up to the brim.
678 Hughes et al. (2020) recently developed a device that allows localized deposition of
679 sedimentary units, opening the way to including detailed sedimentation patterns in
680 analogue models. Another way in which sedimentation can affect a rift system is by the
681 formation of layers with different properties, creating rheological variations and
682 compositional inheritances. The most extreme case is the formation of thick salt
683 deposits, which can decouple the sedimentary cover from the underlying basement, as
684 modelled by many researchers (e.g. McClay et al. 1998, Brun & Fort 2004, Fort et al.
685 2004, Vendeville 2005; Adam & Krezsek 2012, Ge et al. 2019, Fig. 3e). It may be
686 noted that such work is of great interest for hydrocarbon exploration.
687
- 688 (5) The kinematics of rifting concern factors as extension directions, deformation rates, but
689 also changes in general deformation style on the path from incipient rifting to
690 continental break-up. Analogue models are well-suited for studying these topics,
691 especially when addressing their 3D aspects (Figs. 4-8). An interesting challenge may
692 concern extension boundary conditions since extension rates are also known to
693 change over time, especially before the moment of break-up, as shown by Brune et al.
694 (2016). The authors attribute this effect to the fact that the forces that act on a rifting
695 plate are rather constant, but that the dwindling strength of the lithosphere towards
696 break-up translates in a rapid acceleration of extension. Analogue modellers should
697 attempt to incorporate such changing strain rates, at least when modelling large-scale
698 rift systems. This could be done by either programming different extension velocities
699 over time, or perhaps more elegantly, by applying some sort of force boundary
700 condition by means of a weight-and-pulley system. Also here, a link with numerical
701 models may help to explore kinematic links with the deep earth and large-scale driving
702 forces.
703
- 704 (6) Finally, the influence of the mantle, which is considered a dominant factor during rifting
705 and continental break-up should be further explored. This topic is strongly associated
706 with rheology and kinematics, and various analogue modellers have included the
707 mantle in their lithospheric-scale experiments (e.g. Fig. 5, Corti et al. 2003 and
708 references therein). For these models, the inclusion of convenient analogue materials
709 that can mimic temperature-dependent rheological changes during rifting should be a
710 major objective. Furthermore, most lithospheric-scale models have focused on the 2D

711 aspects of rifting. Fully 3D efforts including oblique or rotational rifting such as applied
712 in the works by Agostini et al. (2009), Philippon et al. (2015), and Molnar et al. (2017)
713 will yield important insights on mantle influence within rift systems. Especially the
714 application of advanced methods like CT-scanning and DVC analysis would greatly
715 help to unravel the complex internal deformation of the lithosphere and the interactions
716 between the (different components of the) crust, lithospheric mantle and the
717 asthenosphere below.

718
719 In addition to the research focus points listed above, we must stress that considerable
720 opportunities lie in rerunning models from previous studies. In a first step this would allow to
721 evaluate experimental reproducibility, although this might be challenging as older publications
722 often lack the necessary background information on rheology, set-up and the practicalities
723 surrounding model construction. It is therefore of great importance to provide all relevant
724 information when publishing modelling work (Zwaan et al. 2019) and to make extensive
725 supplementary material public available via online repositories (e.g. at GFZ Data Services,
726 which is part of the EPOS network: <http://dataservices.gfz-potsdam.de>). In a second step,
727 rerunning previously published models would help to obtain more detailed and quantified
728 insights, especially on the evolution of internal model deformation. In fact, models analysed
729 with state-of-the-art PIV, DIC and DVC methods provide a wealth of data, revealing processes
730 and details, as well as boundary effects that may have gone previously unnoticed (e.g. Adam
731 & Krezsec 2012; Molnar et al. 2017; Zwaan et al. 2018, 2020). It is especially this kind of
732 detailed observations made possible by the latest technical developments that constantly help
733 us to revise and improve our interpretations of the natural world.

734
735

736 **Acknowledgements**

737
738 We thank the members of the Tectonics research group of the University of Bern's Institute of
739 Geological Sciences, in particular Marco Herwegh, Veronica Peverelli, Timothy Schmid,
740 Renata Schmitt, James Gilgannon, Vénice Akker and Ferdinando Musso Piantelli, for providing
741 valuable and constructive feedback that greatly helped to improve the text.

742
743
744
745
746

747 **References**

- 748
- 749 Abdelmalak, M.M., Bulois, C., Mourges, R., Galland, O., Legland, J.-B., Gruber, C. 2016.
750 Description of new dry granular materials of variable cohesion and friction coefficient:
751 Implications for laboratory modeling of the brittle crust. *Tectonophysics* 684, 39-51.
752 <https://doi.org/10.1016/j.tecto.2016.03.003>
753
- 754 Acocella, V., Faccenna, C., Funiciello, R., Rossetti, F. 1999. Sand-box modelling of
755 basement-controlled transfer zones in extensional domains. *Terra Nova* 11, 149–156.
756 <https://doi.org/10.1046/j.1365-3121.1999.00238.x>
757
- 758 Agostini, A., Corti, G., Zeoli, A., Mulugeta, G. 2009. Evolution, pattern, and partitioning of
759 deformation during oblique continental rifting: Inferences from lithospheric-scale centrifuge
760 models. *Geochemistry, Geophysics, Geosystems* 10, Q11015.
761 <https://doi.org/10.1029/2009GC002676>
762
- 763 Adam, J., Urai, J.L., Wieneke, B., Oncken, O., Pfeiffer, K., Kukowski, N., Lohrmann, J., Hoth,
764 S., van der Zee, W., Schmatz, J. 2005. Shear localisation and strain distribution during
765 tectonic faulting – new insights from granular-flow experiments and high-resolution optical
766 image correlation techniques. *Journal of Structural Geology*, 27, 283-301.
767 <https://doi.org/10.1016/j.jsg.2004.08.008>
768
- 769 Adam, J., Krezsec, C. 2012. Basin-scale salt tectonic processes of the Laurentian Basin,
770 Eastern Canada: insights from integrated regional 2D seismic interpretation and 4D physical
771 experiments. In: Alsop, G.I., Archer, S.G., Hartley, A.J., Grant, N.T., Hodgkinson, R. (eds) *Salt*
772 *Tectonics, Sediments and Prospectivity*. Geological Society, London, Special Publications,
773 363, 331-360.
774 <http://dx.doi.org/10.1144/SP363.15>
775
- 776 Adam, J., Klinkmüller, M., Schreurs, G., Wieneke, B. 2013. Quantitative 3D strain analysis in
777 analogue experiments simulating tectonic deformation: Integration of X-ray computed
778 tomography and digital volume correlation techniques. *Journal of Structural Geology* 55, 127-
779 149.
780 <https://doi.org/10.1016/j.jsg.2013.07.011>
781
- 782 Allemand, P., Brun, J.-P., Davy, P., Van der Driessche, J. 1989. Symétrie et asymétrie des
783 rifts et mécanismes d'amincissement de la lithosphère. *Bulletin de la Société Géologique de*
784 *France* 8, 445–451.
785 <https://doi.org/10.2113/gssgfbull.V.3.445>
786
- 787 Allemand, P., Brun, J.-P. 1991. Width of continental rifts and rheological layering of the
788 lithosphere. *Tectonophysics* 188, 63-69.
789 [https://doi.org/10.1016/0040-1951\(91\)90314-I](https://doi.org/10.1016/0040-1951(91)90314-I)
790
- 791 Autin, J., Bellahsen, N., Husson, L., Beslier, M.-O. Leroy, S., d'Acremont, E. 2010. Analog
792 models of oblique rifting in a cold lithosphere. *Tectonics* 29, TC6016.
793 <https://doi.org/10.1029/2010TC002671>
794
- 795 Autin, J., Bellahsen, N., Leroy, S., Husson, L., Beslier, M.-O., d'Acremont, E. 2013. The role of
796 structural inheritance in oblique rifting: Insights from analogue models and application to the
797 Gulf of Aden. *Tectonophysics* 607, 51-64.
798 <http://dx.doi.org/10.1016/j.tecto.2013.05.041>
799
- 800 Bahroudi, A., Koyi, H. A., Talbot, C. J. 2003. Effect of ductile and frictional décollements on
801 style of extension. *Journal of Structural Geology* 25, 1401–1423.
802 [https://doi.org/10.1016/S0191-8141\(02\)00201-8](https://doi.org/10.1016/S0191-8141(02)00201-8)
803

804 Benes, V., Scott, S.D. 1996. Oblique Rifting in the Havre Trough and Its Propagation into the
805 Continental Margin of New Zealand: Comparison with Analogue Experiments. *Marine*
806 *Geophysical Researches* 18, 189-201.
807 <https://doi.org/10.1007/BF00286077>
808

809 Beniest, A., Willingshofer, E., Sokoutis, D., Sassi, W. 2018. Extending Continental Lithosphere
810 With Lateral Strength Variations: Effects on Deformation Localization and Margin Geometries.
811 *Frontiers in Earth Science* 6, 148.
812 <https://doi.org/10.3389/feart.2018.00148>
813

814 Bellahsen, N., Daniel, J.-M., Bollinger, L., Burov, E. 2003. Influence of viscous layers on the
815 growth of normal faults: insights from experimental and numerical models. *Journal of*
816 *Structural Geology* 25, 1471-1485.
817 [https://doi.org/10.1016/S0191-8141\(02\)00185-2](https://doi.org/10.1016/S0191-8141(02)00185-2)
818

819 Bellahsen, N., Daniel, J.M. 2005. Fault reactivation control on normal fault growth: an
820 experimental study. *Journal of Structural Geology* 27, 769-780.
821 <https://doi.org/10.1016/j.jsg.2004.12.003>
822

823 Beslier, M.-O. 1991. Formation des marges passives et remontée du manteau: modelisation
824 experimentale et exemple de la marge de la Galice. *Mémoires de Géosciences Rennes*, 45.
825 <https://tel.archives-ouvertes.fr/tel-00594598>
826

827 Bonini, M. Souriot, T., Boccaletti, M., Brun, J.P. 1997. Successive orthogonal and oblique
828 extension episodes in a rift zone: Laboratory experiments with application to the Ethiopian
829 Rift. *Tectonics*, 16, 347– 362.
830 <https://doi.org/10.1029/96TC03935>
831

832 Boutelier, D., Oncken, O. 2011. 3-D thermo-mechanical laboratory modeling of plate-
833 tectonics: modeling scheme, technique and first experiments. *Solid Earth* 2, 35–51.
834 <https://doi.org/10.5194/se-2-35-2011>
835

836 Boutelier, D., Schrank, C., Regenauer-Lieb, K. 2019. 2-D finite displacements and strain from
837 particle imaging velocimetry (PIV) analysis of tectonic analogue models with TecPIV. *Solid*
838 *Earth* 10, 1123–1139.
839 <https://doi.org/10.5194/se-10-1123-2019>
840

841 Brun, J.-P., Sokoutis, D., Van Den Driessche, J. 1994. Analogue modeling of detachment fault
842 systems and core complexes. *Geology* 22, 319-322.
843 [https://doi.org/10.1130/0091-7613\(1994\)022<0319:AMODFS>2.3.CO;2](https://doi.org/10.1130/0091-7613(1994)022<0319:AMODFS>2.3.CO;2)
844

845 Brun, J.-P., Beslier, M.O. 1996. Mantle exhumation at passive margins. *Earth and Planetary*
846 *Science Letters* 142, 161-173.
847 <https://doi.org/10.1051/bsgf/2019007>
848

849 Brun, J.-P , Nalpas, T . 1996. Graben inversion in nature and experiments. *Tectonics* 15 (2),
850 677-687.
851 <https://doi.org/10.1029/95TC03853>
852

853 Brun, J.-P. 1999. Narrow rifts versus wide rifts: inferences for the mechanics of rifting from
854 laboratory experiments. *Philosophical Transactions of the Royal Society of London, A* 357,
855 695-710.
856 <https://doi.org/10.1098/rsta.1999.0349>
857

858 Brun, J.-P. 2002. Deformation of the continental lithosphere: Insights from brittle-ductile
859 models. In: De Meer, S., Drury, M.R., De Bresser, J.H.P., Pennoch, G.M. (eds) *Deformation*

860 Mechanisms, Rheology and Tectonics. Current Status and Future Perspectives. Geological
861 Society, London, Special Publications, 200, 355-370.
862 <https://doi.org/10.1144/GSL.SP.2001.200.01.20>
863
864 Brun, J.-P., Fort, X. 2004. Compressional salt tectonics (Angolan margin). *Tectonophysics*
865 382, 129-150.
866 <https://doi.org/10.1016/j.tecto.2003.11.014>
867
868 Brune, J.N., Ellis, M.A. 1997. Structural features in a brittle–ductile wax model of continental
869 extension. *Nature* 387, 67–70.
870 <https://doi.org/10.1038/387067a0>
871
872 Brune, S., Williams, S., Butterworth, N., Müller, D. 2016. Abrupt plate accelerations shape
873 rifted continental margins. *Nature* 536, 201–204.
874 <https://doi.org/10.1038/nature18319>
875
876 Brune, S., Corti, G., Ranalli, G. 2017. Controls of inherited lithospheric heterogeneity on rift
877 linkage: Numerical and analogue models of interaction between the Kenyan and Ethiopian
878 rifts across the Turkana depression. *Tectonics* 36, 1767-1786.
879 <https://doi.org/10.1002/2017TC004739>
880
881 Brune, S., Williams, S.E., Müller, R.D. 2018. Oblique rifting: the rule, not the exception. *Solid*
882 *Earth* 9, 1187-1206.
883 <https://doi.org/10.5194/se-9-1187-2018>
884
885 Buiter, S.J.H., Babeyko, A.Y., Ellis, S., Gerya, T.V., Kaus, B.J.P., Kellner, A., Schreurs, G.,
886 Yamada, Y. 2006. The numerical sandbox: comparison of model results for a shortening
887 and an extension experiment. In: Buiter, S.J.H., Schreurs, G. (eds) *Analogue and Numerical*
888 *Modelling of Crustal-Scale Processes*. Geological Society, London, Special Publications 253,
889 29–64.
890 <https://doi.org/10.1144/GSL.SP.2006.253.01.02>
891
892 Cerca, M., Ferrari, L, Corti, G., Bonini, M., Manetti, P. 2010. Analogue model of inversion
893 tectonics explaining the structural diversity of Late Cretaceous shortening in southwestern
894 Mexico. *Lithosphere* 2, 172-187.
895 <https://doi.org/10.1130/L48.1>
896
897 Chattopadhyay, A., Chakra, M. 2012. Influence of pre-existing pervasive fabrics on fault
898 patterns during orthogonal and oblique rifting: An experimental approach. *Marine and*
899 *Petroleum Geology* 39, 74-91.
900 <http://dx.doi.org/10.1016/j.marpetgeo.2012.09.009>
901
902 Chauvin, B., Lovely, P., Stockmeyer, J., Plesch, A., Caumon, G., Shaw, J.H. 2018. Validating
903 novel boundary conditions for three-dimensional mechanics-based restoration: An extensional
904 sandbox model example. *AAPG Bulletin* 102, 245-266.
905 <https://doi.org/10.1306/0504171620817154>
906
907 Chemenda, A., Déverchère, J., Calais, E. 2002. Three-dimensional laboratory modelling of
908 rifting: application to the Baikal Rift, Russia. *Tectonophysics* 356, 253-273.
909 [https://doi.org/10.1016/S0040-1951\(02\)00389-X](https://doi.org/10.1016/S0040-1951(02)00389-X)
910
911 Clifton, A.E., Schlische, R.W., Withjack, M.O., Ackermann, R.V. 2000. Influence of rift obliquity
912 on fault-population systematics: results of experimental clay models. *Journal of Structural*
913 *Geology* 22, 1491-1509.
914 [https://doi.org/10.1016/S0191-8141\(00\)00043-2](https://doi.org/10.1016/S0191-8141(00)00043-2)
915

916 Colletta, B., Letouzey, J., Pinedo, R., Ballard, J.F., Balé, P. 1991. Computerized X-ray
917 tomography analysis of sandbox models: Examples of thin-skinned thrust systems. *Geology*
918 19, 1063-1067.
919 [https://doi.org/10.1130/0091-7613\(1991\)019<1063:CXRTAO>2.3.CO;2](https://doi.org/10.1130/0091-7613(1991)019<1063:CXRTAO>2.3.CO;2)
920

921 Corbi, F., Funiciello, F., Moroni, M., Van Dinther, Y., Mai, P.M., Dalguer, L.A., Facenna, C.
922 2013. The seismic cycle at subduction thrusts: 1. Insights from laboratory models. *Journal of*
923 *Geophysical Research: Solid Earth* 118, 1483-1501.
924 <https://doi.org/10.1029/2012JB009481>
925

926 Corbi, F., Sandri, L., Bedford, J., Funiciello, F., Brizzi, S., Rosenau, M., Lallemand, S. 2019.
927 Machine Learning Can Predict the Timing and Size of Analog Earthquakes. *Geophysical*
928 *Research Letters* 46, 1303-1311.
929 <https://doi.org/10.1029/2018GL081251>
930

931 Corti, G., Bonini, B., Conticelli, S., Innocenti, F., Manetti P., Sokoutis, D. 2003. Analogue
932 modelling of continental extension: a review focused on the relations between the patterns of
933 deformation and the presence of magma. *Earth-Science Reviews* 63, 169-247.
934 [https://doi.org/10.1016/S0012-8252\(03\)00035-7](https://doi.org/10.1016/S0012-8252(03)00035-7)
935

936 Corti, G., Van Wijk, J., Cloetingh, S., Morley, C.K. 2007. Tectonic inheritance and continental
937 rift architecture: Numerical and analogue models of the East African Rift system. *Tectonics* 26,
938 TC6006.
939 <https://doi.org/10.1029/2006TC002086>
940

941 Corti, G. 2012. Evolution and characteristics of continental rifting: Analog modeling-inspired
942 view and comparison with examples from the East African Rift System. *Tectonophysics* 522–
943 523,1–33.
944 <https://doi.org/10.1016/j.tecto.2011.06.010>
945

946 Dauteuil, O., Bourgeois, O., Mauduit, T. 2002. Lithosphere strength controls oceanic trans-
947 form zone structure: insights from analogue models. *Geophysical Journal International* 150,
948 706-714.
949 <https://doi.org/10.1046/j.1365-246X.2002.01736.x>
950

951 Donnadieu, F., Kelfoun, K., Van Wijk de Vries, B., Cecchi, E., Merle, O. 2003. Digital
952 photogrammetry as a tool in analogue modelling: applications to volcano instability. *Journal of*
953 *Volcanology and Geothermal Research* 123, 161-180.
954 [https://doi.org/10.1016/S0377-0273\(03\)00034-9](https://doi.org/10.1016/S0377-0273(03)00034-9)
955

956 Dooley, T., McClay, K.R., Pascoe, R. 2003. 3D analogue models of variable displacement
957 extensional faults: applications to the Revfallet Fault system, offshore mid-Norway. In:
958 Nieuwland, D.A. (ed). *New Insights into Structural Interpretation and Modelling*. Geological
959 Society, London, Special Publications, 212, 151-167.
960 <https://doi.org/10.1144/GSL.SP.2003.212.01.10>
961

962 Dooley, T., Schreurs, G. 2012. Analogue modelling of intraplate strike-slip tectonics: A review
963 and new experimental results. *Tectonophysics* 574–575, 1–71
964 <http://dx.doi.org/10.1016/j.tecto.2012.05.030>
965

966 Dooley, T., Hudec, M.R. 2020. Extension and Inversion of Salt-Bearing Rift Systems.
967 *Solid Earth Discussions* (preprint)
968 <https://doi.org/10.5194/se-2020-3>
969

970 Eisenstadt, G., Sims, D. 2005. Evaluating sand and clay models: do rheological differences
971 matter? *Journal of Structural Geology* 27, 1399-1412.
972 <https://doi.org/10.1016/j.jsg.2005.04.010>

973
974 Fedorik, J., Zwaan, F., Schreurs, G., Toscani, G., Bonini, L., Seno, S. 2019. The interaction
975 between strike-slip dominated fault zones and thrust belt structures: Insights from 4D
976 analogue models. *Journal of Structural Geology* 122, 89-105.
977 <https://doi.org/10.1016/j.jsg.2019.02.010>
978
979 Fort, X., Brun, J.-P., Chauvel F. 2004. Salt tectonics on the Angolan margin, synsedimentary
980 deformation processes. *AAPG Bulletin* 88, 1523-1544.
981
982 Ge, Z., Rosenau, M, Warsitzka, M., Gawthorpe, R.L. 2019. Overprinting translational domains
983 in passive margin salt basins: insights from analogue modelling. *Solid Earth* 10, 1283–1300.
984 <https://doi.org/10.5194/se-10-1283-2019>
985
986 Glerum, A., Brune, S., Stamps, D.S., Strecker, M.R. 2020. Victoria continental microplate
987 dynamics controlled by the lithospheric strength distribution of the East African Rift. *Nature*
988 *Communications*.
989 **NO DOI YET**
990
991 Gravelau, F., Malavieille, J., Dominguez, S. 2012. Experimental modelling of orogenic
992 wedges: A review. *Tectonophysics* 538-540, 1–66
993 <https://doi.org/10.1016/j.tecto.2012.01.027>
994
995 Hall, J. Sir. 1815. On the vertical position and convolutions of certain strata and their relation
996 with granite. *Royal Society of Edinburgh Transactions*, 7, 79-108.
997 <https://doi.org/10.1017/S0080456800019268>
998
999 Hubbert, M.K. 1937. Theory of scaled models as applied to the study of geological structures.
1000 *Geological Society of America Bulletin* 48, 1459-1520.
1001
1002 Hughes, A., Adam, J., Burgess, P. 2020. Integrating analogue and numerical modelling
1003 techniques for improved simulation of coupled regional tectonic processes and syn-
1004 depositional systems. *EGU General Assembly*. EGU2020-5059
1005 <https://doi.org/10.5194/egusphere-egu2020-5059>
1006
1007 Holland, M., Urai, J.L., Martel, S. 2006. The internal structure of fault zones in basaltic
1008 sequences. *Earth and Planetary Science Letters* 248, 286–300.
1009 <https://doi.org/10.1016/j.epsl.2006.05.035>
1010
1011 Jackson, C.A.-L., Bell, R.E., Torevatn, A., Tvedt, A.B.M. 2017. Techniques to determine the
1012 kinematics of synsedimentary normal faults and implications for fault growth models. In:
1013 Childs, C., Holdsworth, R.E., Jackson, C.A.-L., Manzocchi, T., Walsch, J.J., Yielding, G. (eds).
1014 *The Geometry and Growth of Normal Faults*. Geological Society, London, Special Publications
1015 439.
1016 <https://doi.org/10.1144/SP439.22>
1017
1018 Katz, R.F., Ragnarsson, R., Bodenschatz, E., 2005. Tectonic microplates in a wax model of
1019 sea-floor spreading. *New Journal of Physics* 7, 37
1020 <https://doi.org/10.1088/1367-2630/7/1/037>
1021
1022 Keep, M., McClay, K.R. 1997. Analogue modelling of multiphase rift systems. *Tectonophysics*
1023 273, 239-270.
1024 [https://doi.org/10.1016/S0040-1951\(96\)00272-7](https://doi.org/10.1016/S0040-1951(96)00272-7)
1025
1026 Klinkmüller, M., Schreurs, G., Rosenau, M., Kemnitz, H. 2016. Properties of granular
1027 analogue model materials: A community wide survey, *Tectonophysics*, 684, 23–38,
1028 <https://doi.org/10.1016/j.tecto.2016.01.017>
1029

1030 Koyi, H. 1997. Analogue modelling: From a qualitative to a quantitative technique – a historical
1031 outline. *Journal of Petroleum Geology* 20, 223-238.
1032 <https://doi.org/10.1130/GSAB-48-1459>
1033

1034 Le Calvez, J.H. 2002. Physical modelling of normal faults and graben relays above salt. PhD
1035 Thesis, University of Texas, Austin.
1036 <http://hdl.handle.net/2152/11057>
1037

1038 Le Calvez, J.H., Vendeville, B.C. 2002. Experimental designs to model along-strike fault
1039 interaction. In: Schellart, W.P., Passchier, C. (eds.) *Analogue modelling of large-scale*
1040 *tectonic processes. Journal of the Virtual Explorer* 7, 1-17.
1041 <https://doi.org/10.3809/jvirtex.2002.00043>
1042

1043 Lindanger, R., Øygaren, M., Gabrielsen, R.H., Mjelde, R., Randen, T., Tjøstheim, B.A. 2004.
1044 Analogue (plaster) modelling and synthetic seismic representation of hangingwall fault blocks
1045 above ramp-flat ramp extensional faults. *First Break* 22, 33-41.
1046 <http://old.earthdoc.org/publication/publicationdetails?publication=25747>
1047

1048 Martí, J., Geyer, A., Folch, A., Gottsmann, J. 2008. A Review on Collapse Caldera Modelling.
1049 In: Gottsmann, J., Martiacute, J. *Caldera Volcanism: Analysis, Modelling and Response.*
1050 *Developments in Volcanology* 10, 233-283
1051 [https://doi.org/10.1016/S1871-644X\(07\)00006-X](https://doi.org/10.1016/S1871-644X(07)00006-X)
1052

1053 Martin, A.K. 1984. Propagating rifts: Crustal extension during continental rifting. *Tectonics* 3,
1054 611-617.
1055 <https://doi.org/10.1029/TC003i006p00611>
1056

1057 Mattioni, L., Sassi, W., Callot, J.-P. 2007 Analogue models of basin inversion by
1058 transpression: role of structural heterogeneity. In: Ries, A.C., Butler, R.W.H., Graham, R.H.
1059 (eds). *Deformation of the Continental Crust. The Legacy of Mike Coward.* Geological Society,
1060 London, Special Publications, 272, 3974 17.
1061 <https://doi.org/10.1144/GSL.SP.2007.272.01.20>
1062

1063 McClay, K.R. 1990. Extensional fault systems in sedimentary basins: a review of analogue
1064 model studies. *Marine and Petroleum Geology* 7, 206-233.
1065 [https://doi.org/10.1016/0264-8172\(90\)90001-W](https://doi.org/10.1016/0264-8172(90)90001-W)
1066

1067 McClay, K.R., White, M.J. 1995. Analogue modelling of orthogonal and oblique rifting. *Marine*
1068 *and Petroleum Geology* 12, 137- 151.
1069 [https://doi.org/10.1016/0264-8172\(95\)92835-K](https://doi.org/10.1016/0264-8172(95)92835-K)
1070

1071 McClay, K.R. 1996. Recent advances in analogue modelling: uses in section interpretation
1072 and validation. In: Buchanan, E.G., Nieuwland, D.A. (eds). *Modern Developments in Structural*
1073 *Interpretation, Validation and Modelling.* Geological Society Special Publications 99, 201-225.
1074 <https://doi.org/10.1144/GSL.SP.1996.099.01.16>
1075

1076 McClay, K.R., Dooley, T., Lewis, G. 1998. Analog modeling of progradational delta systems.
1077 *Geology* 26, 771-774.
1078 [https://doi.org/10.1130/0091-7613\(1998\)026<0771:AMOPDS>2.3.CO;2](https://doi.org/10.1130/0091-7613(1998)026<0771:AMOPDS>2.3.CO;2)
1079

1080 McClay, K.R., Dooley, T., Whitehouse, P., Mills, M. 2002. 4-D evolution of rift systems:
1081 Insights from scaled physical models. *AAPG Bulletin* 86, 935-959.
1082 <https://doi.org/10.1306/61EEDBF2-173E-11D7-8645000102C1865D>
1083

1084 McFall, B.C., Fritz, H.M. 2016 Physical modelling of tsunamis generated by three-dimensional
1085 deformable granular landslides on planar and conical island slopes. *Proceedings of the Royal*
1086 *Society A* 472, 20160052.

1087 <http://dx.doi.org/10.1098/rspa.2016.0052>
1088
1089 Michon, L., Merle, O. 2000. Crustal structures of the Rhinegraben and the Massif Central
1090 grabens: An experimental approach. *Tectonics* 19, 896-904.
1091 <https://doi.org/10.1029/2000TC900015>
1092
1093 Michon, L., Merle, O. 2003. Mode of lithospheric extension: Conceptual models from analogue
1094 modeling. *Tectonics* 22, 1028.
1095 <https://doi.org/10.1029/2002TC001435>
1096
1097 Michon, L., Sokoutis, D. 2005. Interaction between structural inheritance and extension
1098 direction during graben and depocentre formation: An experimental approach. *Tectonophysics*
1099 409, 125-146.
1100 <https://doi.org/10.1016/j.tecto.2005.08.020>
1101
1102 Molnar, N.E., Cruden, A.R., Betts, P.G. 2017. Interactions between propagating rotational rifts
1103 and linear rheological heterogeneities: Insights from three-dimensional laboratory
1104 experiments. *Tectonics* 36, 420-443.
1105 <https://doi.org/10.1002/2016TC004447>
1106
1107 Molnar, N.E., Cruden, A.R., Betts, P.G. 2018. Unzippingg continents and the birth of
1108 microcontinents. *Geology* 46, 451–454
1109 <https://doi.org/10.1130/G40021.1>
1110
1111 Molnar, N.E., Crusden, A. R., Betts, P.G. 2019. Interactions between propagating rifts and
1112 linear weaknesses in the lower crust. *Geosphere* 15, 1617-1640.
1113 <https://doi.org/10.1130/GES02119.1>
1114
1115 Montanari, D., Agostini, A., Bonini, M., Corti, G., Del Ventisette, C., 2017. The Use of
1116 Empirical Methods for Testing Granular Materials in Analogue Modelling. *Materials* 10, 635.
1117 <https://doi.org/10.3390/ma10060635>
1118
1119 Naylor, M.A., Mandl, G., Sijpesteijn, C.H.K. 1986. Fault geometries in basement-induced
1120 wrench faulting under different initial stress states. *Journal of Structural Geology* 8, 737-752.
1121 [https://doi.org/10.1016/0191-8141\(86\)90022-2](https://doi.org/10.1016/0191-8141(86)90022-2)
1122
1123 Naylor, M.A., Laroque, J.M., Gauthier, B.D.M. 1994. Understanding extensional tectonics:
1124 insights from sandbox models. Roure, F.; Ellouz, N.; Shein, V.S.; Skvortsov, I.I. (eds).
1125 Geodynamic evolution of sedimentary basins. International Symposium on Geodynamic
1126 Evolution of Sedimentary Basins, Moscow (Russian Federation). Technip, 92 (France), 69-83.
1127
1128 Nestola, Y., Storti, F., CavoZZi, C. 2015. Strain rate-dependent lithosphere rifting and necking
1129 architectures in analog experiments. *Journal of Geophysical Research: Solid Earth* 120, 584-
1130 594.
1131 <https://doi.org/10.1002/2014JB011623>
1132
1133 Oldenburg, D.W., Brune, J.N. 1972. Ridge Transform Fault Spreading Pattern in Freezing
1134 Wax. *Science* 178, 301-304.
1135 <https://doi.org/10.1126/science.178.4058.301>
1136
1137 Panien, M., Schreurs, G, Pfiffner, A. 2005. Sandbox experiments on basin inversion: testing
1138 the influence of basin orientation and basin fill. *Journal of Structural Geology* 27, 433-445.
1139 <https://doi.org/10.1016/j.jsg.2004.11.001>
1140
1141 Panien, M., Schreurs, G, Pfiffner, A. 2006(a). Mechanical behaviour of granular materials
1142 used in analogue modelling: insights from grain characterisation, ring-shear tests and
1143 analogue experiments. *Journal of Structural Geology* 28, 1710-1724.

1144 <https://doi.org/10.1016/j.jsg.2006.05.004>
1145
1146 Panien, M., Buiter, S.J.H., Schreurs, G., Pfiffner, O.A. 2006(b). Inversion of a symmetric basin:
1147 insights from a comparison between analogue and numerical experiments. In: Buiter, S.J.H.,
1148 Schreurs, G. (eds). *Analogue and Numerical Modelling of Crustal-Scale Processes*. Geological
1149 Society, London, Special Publications 253, 253-270.
1150 <https://doi.org/10.1144/GSL.SP.2006.253.01.13>
1151
1152 Peron-Pinvidic, G., Manatschal, G., “IMAGinING RIFTING” Workshop Participants. 2019.
1153 *Rifted Margins: State of the Art and Future Challenges*. *Frontiers in Earth Sciences* 7, 208
1154 <https://doi.org/10.3389/feart.2019.00218>
1155
1156 Philippon, M., Willingshofer, E., Sokoutis, D., Corti, G., Sani, F., Bonini, M., Cloetingh, S.
1157 2015. Slip re-orientation in oblique rifts. *Geology* 43, 147-150.
1158 <https://doi.org/10.1130/G36208.1>
1159
1160 Poppe, S., Holohan, E.P., Galland, O., Buls, N., Van Gompel, G., Keelson, B., Tournigand, P.-
1161 Y., Brancart, J., Hollis, D., Nila, A., Kervyn, M. An Inside Perspective on Magma Intrusion:
1162 Quantifying 3D Displacement and Strain in Laboratory Experiments by Dynamic X-Ray
1163 Computed Tomography. *Frontiers in Earth Science* 7, 62.
1164 <https://doi.org/10.3389/feart.2019.00062>
1165
1166 Quirk, D.G., Schødt, N., Lassen, B., Ings, S.J., Hsu, D., Hirsch, K.K., Von Nicolai, C. 2012.
1167 Salt tectonics on passive margins: examples from Santos, Campos and Kwanza basins. In:
1168 Alsop, G.I., Archer, S.G., Hartley, A.J., Grant, N.T., Hodgkinson, R. (eds). *Salt Tectonics,*
1169 *Sediments and Prospectivity*. Geological Society, London, Special Publications 363, 207 –
1170 244.
1171 <http://dx.doi.org/10.1144/SP363.10>
1172
1173 Ramberg, H. 1981. *Gravity, Deformation and the Earth’s Crust*. Academic Press, London.
1174
1175 Reber, J., Cooke, M.L. Dooley, T.P. 2020. What model material to use? A Review on rock
1176 analogs for structural geology and tectonics. *Earth-Science Reviews*.
1177 <https://doi.org/10.1016/j.earscirev.2020.103107>
1178
1179 Ritter, M.C., Leever, K., Rosenau, M., Oncken, O. 2016. Scaling the sandbox—Mechanical
1180 (dis) similarities of granular materials and brittle rock. *Journal of Geophysical Research: Solid*
1181 *Earth* 121, 6863-6879.
1182 <https://doi.org/10.1002/2016JB012915>
1183
1184 Rudolf, M., Boutelier, D., Rosenau, M., Schreurs, G., Oncken, O. 2016. Rheological
1185 benchmark of silicone oils used for analog modeling of short- and long-term lithospheric
1186 deformation, *Tectonophysics* 684, 12–22
1187 <https://doi.org/10.1016/j.tecto.2015.11.028>
1188
1189 Schellart, W.P., Strak, V. 2016. A review of analogue modelling of geodynamic processes:
1190 Approaches, scaling, materials and quantification, with an application to subduction
1191 experiments, *J. Geodyn.*, 100, 7–32.
1192 <https://doi.org/10.1016/j.jog.2016.03.009>
1193
1194 Schlagenhauf, A., Dominguez, S., Malavieille, J., Manighetti, I. 2008. Incremental growth of
1195 normal faults: Insights from a laser-equipped analog experiment. *Earth and Planetary Science*
1196 *Letters* 273, 299–311.
1197 <https://doi.org/10.1016/j.epsl.2008.06.042>
1198
1199 Schreurs, G., Hänni, R., Panien, M., Vock, P. 2003. Analysis of analogue models by helical X-
1200 ray computed tomography. In: Mees, F., Swennen, R., Van Geet, M., Jacobs, P. *Applications*

1201 of X-ray Computed Tomography in the Geosciences. Geological Society, London, Special
1202 Publications 215, 213-223.
1203 <https://doi.org/10.1144/GSL.SP.2003.215.01.20>
1204
1205 Souriot, T., Brun, J.-P. 1992. Faulting and block rotation in the Afar triangle, East Africa: The
1206 Danakil “crank-arm” model. *Geology* 20, 911-914.
1207 [https://doi.org/10.1130/0091-7613\(1992\)020<0911:FABRIT>2.3.CO;2](https://doi.org/10.1130/0091-7613(1992)020<0911:FABRIT>2.3.CO;2)
1208
1209 Sun., Z., Zhong, Z., Keep, M., Zhou, D., Cai, D., Li, X., Wu, S., Jiang, J. 2009. 3D analogue
1210 modelling of the South China Sea: A discussion on breakup pattern. *Journal of Asian Earth*
1211 *Sciences* 34, 544-556.
1212 <https://doi.org/10.1016/j.jseaes.2008.09.002>
1213
1214 Tentler, T. 2003a. Analogue modeling of overlapping spreading centers: insights into their
1215 propagation and coalescence. *Tectonophysics* 376, 99-115.
1216 <https://doi.org/10.1016/j.tecto.2003.08.011>
1217
1218 Tentler, T. 2003b. Analogue modeling of tension fracture pattern in relation to mid-ocean ridge
1219 propagation. *Geophysical Research Letters* 30, 1268.
1220 <https://doi.org/10.1029/2002GL015741>
1221
1222 Tripanera, D., Acocella, V. Ruch, J. 2014. Dike - induced contraction along oceanic and
1223 continental divergent plate boundaries. *Geophysical Research Letters* 41, 7098-7104.
1224 <https://doi.org/10.1002/2014GL061570>
1225
1226 Tron, V., Brun, J.-P. 1991. Experiments on oblique rifting in brittle-ductile systems.
1227 *Tectonophysics*, 188, 71–88.
1228 [https://doi.org/10.1016/0040-1951\(91\)90315-J](https://doi.org/10.1016/0040-1951(91)90315-J)
1229
1230 Van Mechelen, J.L.M. 2004. Strength of moist sand controlled by surface tension for tectonic
1231 analogue modelling. *Tectonophysics* 384, 275-284.
1232 <https://doi.org/10.1016/j.tecto.2004.04.003>
1233
1234 Vendeville, B., Cobbold, P.R., Davy, P., Brun, J.-P., Choukroune, P. 1987. Physical models
1235 of extensional tectonics at various scales. In: Coward, M.P., Dewey, J.F., Hancock, P.L. (eds.)
1236 *Continental Extensional Tectonics*. Geological Society, London, Special Publications 28, 95-
1237 107.
1238 <https://doi.org/10.1144/GSL.SP.1987.028.01.08>
1239
1240 Vendeville, B.C. 2005. Salt tectonics driven by sediment progradation: Part I—Mechanics and
1241 kinematics. *AAPG Bulletin* 89, 1071-1079.
1242 <https://doi.org/10.1306/03310503063>
1243
1244 Vink, G.E. 1982. Continental Rifting and the Implications For Plate Tectonic Reconstructions.
1245 *Journal of Geophysical Research* 87, 10,667-10,688.
1246 <https://doi.org/10.1029/JB087iB13p10677>
1247
1248 Wang, J., Jiang, Z., Zhang, Y., Gao, L., Wei, X., Zhang, W., Liang, Y., Zhang, H. 2015. Flume
1249 tank study of surface morphology and stratigraphy of a fan delta. *Terra Nova* 27, 42-53.
1250 <https://doi.org/10.1111/ter.12131>
1251
1252 Withjack, M.O., Jamison, W.R. 1986. Deformation produced by oblique rifting. *Tectonophysics*
1253 126, 99-124.
1254 [https://doi.org/10.1016/0040-1951\(86\)90222-2](https://doi.org/10.1016/0040-1951(86)90222-2)
1255

1256 Withjack, M.O., Henza, A.A., Schlische, R.W. 2017. Three-dimensional fault geometries and
1257 interactions within experimental models of multiphase extension. AAPG Bulletin 101, 1767-
1258 1789.
1259 <https://doi.org/10.1306/02071716090>
1260
1261 Wu, J.E., McClay, K., Whitehouse, P., Dooley, T. 2009. 4D analogue modelling of
1262 transtensional pull-apart basins. Marine and Petroleum Geology 26, 1608-1623.
1263 <https://doi.org/10.1016/j.marpetgeo.2008.06.007>
1264
1265 Zwaan, F., Schreurs, G., Naliboff, J., Buiter, S.J.H. 2016. Insights into the effects of oblique
1266 extension on continental rift interaction from 3-D analogue and numerical models.
1267 Tectonophysics 693, 239–260.
1268 <https://doi.org/10.1016/j.tecto.2016.02.036>
1269
1270 Zwaan, F., Schreurs, G. 2017. How oblique extension and structural inheritance influence rift
1271 segment interaction: Insights from 4D analog models. Interpretation 5, SD119–SD138.
1272 <http://dx.doi.org/10.1190/INT-2016-0063.1>
1273
1274 Zwaan, F., Schreurs, G., Adam, J. 2018. Effects of sedimentation on rift segment evolution
1275 and rift interaction in orthogonal and oblique extensional settings: Insights from analogue
1276 models analysed with 4D X-ray computed tomography and digital volume correlation
1277 techniques. Global and Planetary Change 171, 110– 133.
1278 <https://doi.org/10.1016/j.gloplacha.2017.11.002>
1279
1280 Zwaan, F., Scheurs, G., Buiter, S.J.H. 2019. A systematic comparison of experimental set-ups
1281 for modelling extensional tectonics. Solid Earth 10, 1063-1097.
1282 <https://doi.org/10.5194/se-10-1063-2019>
1283
1284 Zwaan, F., Schreurs, G., Rosenau, M. 2020. Rift propagation in rotational versus orthogonal
1285 extension: Insights from 4D analogue models. Journal of Structural Geology 135
1286 <https://doi.org/10.1016/j.jsg.2019.103946>
1287
1288
1289
1290
1291
1292